Interface Focus

Quantitative contrast-enhanced ultrasound imaging: a review of sources of variability

M.-X. Tang, H. Mulvana, T. Gauthier, A. K. P. Lim, D. O. Cosgrove, R. J. Eckersley and E. Stride

Interface Focus 2011 **1**, doi: 10.1098/rsfs.2011.0026 first published online 18 May 2011

Interface Focus

Interface Focus (2011) **1**, 520–539
doi:10.1098/rsfs.2011.0026
Published online 18 May 2011

Review

Quantitative contrast-enhanced ultrasound imaging: a review of sources of variability

M.-X. Tang[1,*], H. Mulvana[2], T. Gauthier[3], A. K. P. Lim[4], D. O. Cosgrove[2], R. J. Eckersley[2] and E. Stride[5]

[1]*Department of Bioengineering, Imperial College London, London SW7 2AZ, UK*
[2]*Imaging Sciences Department, Faculty of Medicine, Imperial College London, London W12 0HS, UK*
[3]*Department of Experimental Medicine and Toxicology, Hammersmith Hospital, Imperial College London, London W12 0NN, UK*
[4]*Hammersmith Hospital, MRC Clinical Sciences Centre, Faculty of Medicine, Imperial College London, London W12 0NN, UK*
[5]*Department Mechanical Engineering, University College London, London WC1E 7JE, UK*

Ultrasound provides a valuable tool for medical diagnosis offering real-time imaging with excellent spatial resolution and low cost. The advent of microbubble contrast agents has provided the additional ability to obtain essential quantitative information relating to tissue vascularity, tissue perfusion and even endothelial wall function. This technique has shown great promise for diagnosis and monitoring in a wide range of clinical conditions such as cardiovascular diseases and cancer, with considerable potential benefits in terms of patient care. A key challenge of this technique, however, is the existence of significant variations in the imaging results, and the lack of understanding regarding their origin. The aim of this paper is to review the potential sources of variability in the quantification of tissue perfusion based on microbubble contrast-enhanced ultrasound images. These are divided into the following three categories: (i) factors relating to the scanner setting, which include transmission power, transmission focal depth, dynamic range, signal gain and transmission frequency, (ii) factors relating to the patient, which include body physical differences, physiological interaction of body with bubbles, propagation and attenuation through tissue, and tissue motion, and (iii) factors relating to the microbubbles, which include the type of bubbles and their stability, preparation and injection and dosage. It has been shown that the factors in all the three categories can significantly affect the imaging results and contribute to the variations observed. How these factors influence quantitative imaging is explained and possible methods for reducing such variations are discussed.

Keywords: microbubble contrast agent; medical ultrasound; perfusion quantification; quantitative imaging; variation

1. INTRODUCTION

The ability to image and quantify tissue perfusion is highly desirable in the clinical assessment of a wide range of conditions involving changes to local blood flow such as cancer and cardiovascular diseases. The development of contrast-enhanced ultrasound (CEUS) imaging with microbubble contrast agents has provided a unique means of visualizing and quantifying tissue perfusion, offering significant advantages in terms of real-time imaging, convenience, cost and patient safety [1–4]. A rich body of literature has demonstrated the potential usefulness of this quantitative imaging technique. An example of a CEUS image featuring a hepatocellular carcinoma is shown in figure 1. There remain, however, considerable challenges that need to be addressed before wider clinical uptake of quantitative CEUS imaging can be achieved. These are largely related to the high degree of variability that is sometimes observed in quantitative results and the resulting diagnostic uncertainty. The aim of this paper is to review current understanding of the sources of this variability and potential ways to reduce it. This

*Author for correspondence (mengxing.tang@imperial.ac.uk).

One contribution of 15 to a Theme Issue 'Recent advances in biomedical ultrasonic imaging techniques'.

Received 17 March 2011
Accepted 26 April 2011

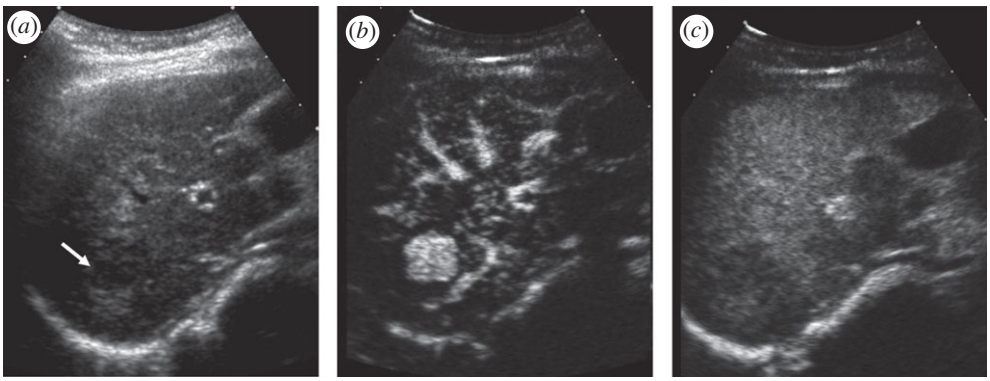

Figure 1. An example of CEUS images featuring a hepatocellular carcinoma detected at surveillance ultrasound in a 60-year-old woman with hepatitis B virus. (*a*) Traditional B-mode sonogram shows a small hypoechoic mass (arrow) in the right lobe of a small cirrhotic liver. (*b*) CEUS image at the peak of arterial phase enhancement shows classic hypervascularity of the tumour. (*c*) CEUS image in the portal venous phase at 2 min; the lesion has washed out relative to the more enhanced liver. Adapted from Wilson & Burns, *Radiology* 257, 24–39, 2010, RSNA©.

Table 1. Summary of some commercial ultrasound contrast agents and their compositions.

agent	manufacturer	coating	gas
SonoVue	Bracco Diagnostics, Inc.	phospholipid	sulphur-hexafluoride
Definity	Lantheus Medical Imaging (formerly Bristol-Myers Squibb, Inc.)	phospholipid	octafluoro-propane
Optison	GE Healthcare	protein (human serum albumin)	octafluoro-propane
Sonazoid	GE Healthcare	lipid	perfluoro-butane
Levoist	Schering	lipid	air
Albunex	Molecular Biosystems/Mallinckrodt	protein (human serum albumin)	air

section will introduce the basic principles of CEUS and identify the key challenges currently being faced.

1.1. Microbubble agents

The development of contrast agents for ultrasound imaging came about as the result of an accidental discovery in the late 1960s that the presence of gas bubbles in the circulation could significantly enhance ultrasound signal intensity [5,6]. Since then, a number of different types of agents have evolved (table 1), all of which generate a suspension of bubbles upon being administered, normally by intravenous injection. The bubbles must be sufficiently small to cross the capillary bed of the pulmonary circulation, and are therefore typically a few micrometres in diameter. In consequence, they are normally referred to as microbubbles. At the same time, these bubbles are big enough that they do not cross the vascular endothelium, making them true intravascular agents. In order to prevent the bubbles from rapidly dissolving and/or agglomerating, they are stabilized by a coating of a biocompatible surfactant or polymer, most commonly phospholipids or proteins. This coating both lowers the interfacial tension at the bubble surface and also provides a barrier to gas diffusion. The nature of the coating also has a significant effect upon the acoustic response of the bubbles, and their physiological interactions *in vivo*, which will be discussed in more detail in §§3 and 4. Despite being similar in size to red blood cells, bubbles are much more efficient scatterers of ultrasound owing to the fact that they are filled with gas and thus highly compressible. Upon ultrasound excitation, they undergo volumetric oscillations and so absorb and reradiate the incident sound rather than merely acting as passive reflectors. There is also a fortunate coincidence in the range of frequencies used for diagnostic ultrasound imaging and that over which bubbles exhibit resonant oscillations. Following injection, the bubbles circulate throughout the vascular space and greatly increase the amplitude of the scattered signals not only from large vessels and cavities but also from the microvasculature, making imaging of tissue perfusion possible.

1.2. Contrast-specific images and time–intensity curves

A key feature of bubble behaviour is that at moderate ultrasound pressure a bubble will oscillate nonlinearly and the backscattered signal consequently contains a range of frequencies in addition to that of the incident ultrasound field. These additional frequency components are usually whole or fractional multiples (harmonics) of the incident frequency. Numerous signal-processing techniques have been developed to exploit this nonlinear behaviour and separate echoes generated by bubbles from those originating from tissue [1]. This kind of technique typically transmits multiple pulses of varying phase or amplitude and can simultaneously produce two images: (i) a conventional B-mode image of the tissue (but slightly downgraded owing to low acoustic power used), and (ii) a contrast-specific image that reflects the spatial distribution of bubbles. The contrast-specific images are formed by

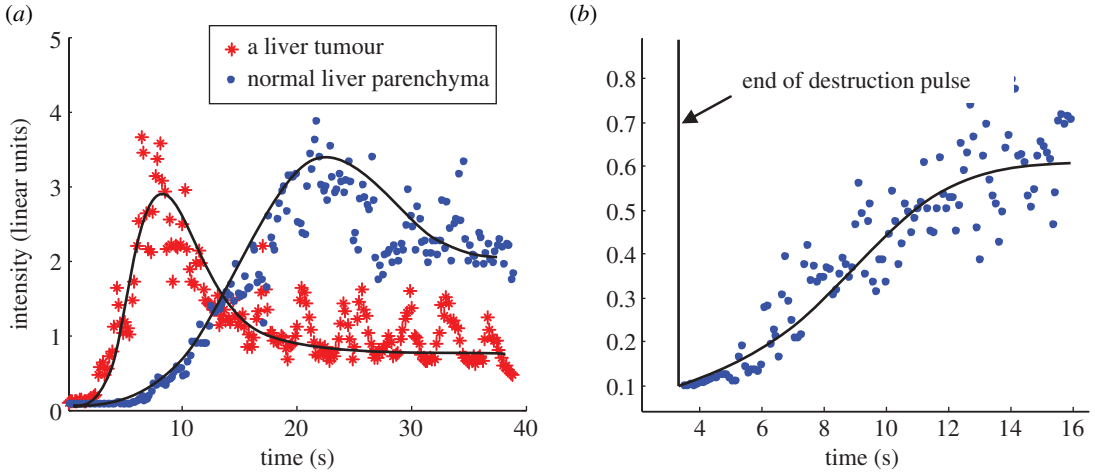

Figure 2. Clinical examples of a TIC for (*a*) a bolus injection in a liver; and (*b*) constant infusion with destruction–replenishment in the myocardium. Oscillations in the signals were mainly caused by tissue motion during imaging, while in (*b*) cardiac systole may also have contributed to the oscillation. Note that the *y*-axes between (*a*) and (*b*) are not comparable as they were acquired with different scanner settings on different patients.

separating the nonlinear signals at various harmonic frequencies from the linear signals at the fundamental frequency. Important examples are pulse inversion (PI), amplitude modulation and the combination of the two [7]. The generation of contrast-specific images forms the basis for quantification of tissue perfusion and for the remainder of this paper, only such contrast-specific images are considered unless otherwise stated.

Since images of bubbles can be formed in real time, a series of contrast-specific images can be obtained and the tissue uptake of the bubbles can thus be observed as a function of time. Quantification is based either on the image intensity or the timing of the tissue uptake of the bubbles. A curve of image intensity versus time (the so-called time–intensity curve (TIC)) can be produced for any pixel or region within the image plane. Two types of TICs can be obtained depending on whether the bubbles are administered as a bolus injection or via a constant infusion. A bolus is relatively simple to administer and more common in clinical practice, while constant infusion is always combined with a 'destruction–replenishment' mode in which higher power ultrasound pulses are used to destroy the bubbles in the imaging plane followed by low-power ultrasound pulses to monitor replenishment in the tissue [8,9]. This technique is unique to ultrasound as no other imaging modalities can deactivate their contrast-enhancing agents to create a new input pulse. Given the noisy nature of the data, models are commonly used to fit the data to remove the noise and extract relevant indices [8,10–12]. Examples of the two types of TIC are shown in figure 2.

From TICs, a number of temporal and amplitude features can be obtained, from which clinically relevant indices such as the fractional vascular volume, flow velocity, relative perfusion rate and transit time etc. can be derived. One can process the images pixel by pixel in this way and generate a map for each of the indices [13,14]. It should be noted that amplitude-derived features are more likely to be affected by system changes than temporally derived features. A number of clinical conditions have been studied, including the diagnosis of liver lesions (see recent reviews by Cosgrove [2] and Wilson [3]) and assessment of myocardial function (see a recent review by Porter [15]). Notably, recent studies have shown great promise in the use of quantitative contrast ultrasound to evaluate tumour therapy [16,17] and assess atherosclerotic lesion neovascularization. [18].

It should be noted that there is another technique that images the transient disruption of microbubbles using the so-called flash imaging [19] or stimulated acoustic emission [20]. Although the disruption of bubbles can greatly enhance the signal amplitude, it is at the cost of transmitting significantly higher amplitude ultrasound, and the tissue background signals also increase significantly. Furthermore, this technique cannot acquire consecutive frames in real time as bubbles must replenish the field of view before the next acquisition. Although this review focuses on the low-power continuous imaging, most of the factors discussed here are still relevant to the high-power transient imaging technique.

1.3. Linear versus logarithmic data

One key underlying assumption for quantification based on TICs is that image intensity is linearly proportional to the concentration of bubbles and thus blood flow. Early studies of quantification relied on video intensity data, to which logarithmic compression had been applied. It has been gradually recognized that linear echo data (sometimes called 'raw data') acquired before compression should be used instead [21,22]. Many ultrasound scanners have their own inbuilt quantification software package, which uses linear echo data to calculate the TIC rather than video intensity. Although linear echo data can also be obtained by reversing the log compression of the video intensity data (this is used by the commercial system SonoLiver Bracco/Tomtek), a direct acquisition before log compression is preferred since the compression process

may cause information loss that cannot be fully recovered by reversing the compression (see §2.3 for further details).

1.4. Challenges

Currently, quantification of tissue perfusion poses considerable challenges. The existence of significant variations in quantitative CEUS results was reported as long ago as 2001 [23,24], but the question has still yet to be fully addressed, and this has prevented this approach from being widely accepted as a clinically useful tool. The variations referred to are caused by factors other than regional blood flow or bubble concentration. For example, different TICs may be obtained from the same region of interest (ROI) in the same subject when scanned at different times if the scanner settings, the position of the probe, the way bubbles are handled or the subject's physiological conditions are different. Even during the same scan, tissues of the same type (and hence similar perfusion profile) may generate different TICs if signals obtained at different depths are not corrected for attenuation and nonlinear propagation. Despite the fact that various normalization and standardization procedures have been used to reduce such variations, they have enjoyed only limited success and require highly experienced operators. We believe that a better understanding of the different sources of variations will facilitate the development of accurate calibration techniques that will lead in turn to improved quantification.

A number of factors may contribute to variability in quantitative CEUS: (i) scanner settings, (ii) patient factors (physiological factors and propagation/attenuation), and (iii) bubble types and handling. This paper will review the current understanding of how each factor influences quantitative imaging and its contribution to measurement variation and discuss potential methods for reduction of the variations.

2. SCANNER SETTINGS

2.1. Output power (mechanical index)

Changes to the transmit amplitude of the ultrasound scanner are indicated by the mechanical index (MI) displayed on the screen. MI is a measure of the potential for mechanical bioeffects (cavitation) in tissue owing to ultrasound exposure and is defined as the peak negative ultrasound pressure in kPa divided by the square root of the ultrasound frequency in MHz. The FDA stipulates a maximum MI of 1.9 in clinical examination, but typically a much lower MI (0.05–0.4) is used for CEUS to minimize bubble disruption. Changes in the amplitude of the transmitted pulse pressure result in changes in the received echo signals and thus alter the amplitude-dependent indices of a derived TIC. A critical question is how much change in the TIC is likely if, for example, the same tissue is scanned with different MIs. If linear proportionality between changes in the MI and changes in TIC amplitude values can be assumed, then simply normalizing the TIC with the applied MI will remove the variations. However, it is well known that bubble behaviour, including both scattering and attenuation, is nonlinear with respect to the ultrasound pressure and hence the MI [25–27]. In order to study the changes in the TICs caused by changes in the MI, a detailed examination of the relationship between bubble behaviour and the driving ultrasound pressure is required. In this section, the nonlinear scattering behaviour of bubbles is examined, while nonlinear attenuation will be discussed in §§3.4 and 3.5. It should be noted that given a certain MI value, the acoustic pressure still varies within the imaging plane owing to tissue attenuation and ultrasound wave diffraction. Hence, the true MI value is spatially variant and the machine-indicated MI only provides a rough estimation at the ultrasound focus.

Morgan *et al.* [28] demonstrated that echo signal power at the second harmonic increases nonlinearly (i.e. non-proportionally) with transmitted ultrasound amplitude for three different contrast agents (Albunex, MP1950 and Optison). They also found significant differences in the acoustic response of the three types of bubbles; nonlinear scattering increased more sharply with Albunex than with Optison at higher pressures (greater than 200 kPa). Shi *et al.* [29,30] investigated subharmonic emissions and showed that for the agents Optison and Levovist, subharmonic generation is highly nonlinear with respect to the incident pressure. They identified three phases as the incident pressure was increased, with the amplitude of the subharmonic component undergoing rapid growth in the intermediate acoustic pressure range ($300 \sim 600$ kPa, 1 atm = 101 kPa), with much slower increases at both lower and higher acoustic pressures. Emmer *et al.* [31] reported a 'threshold' for the behaviour of lipid-shelled bubbles whereby they only start to oscillate above a certain acoustic pressure.

We have measured the PI signals from SonoVue when excited by broadband ultrasound at different acoustic amplitudes. Figure 3 shows the PI signal power normalized by the MI as a function of the MI in both simulation and experiments. It should be noted that the MI is quoted as it is the indication of ultrasound amplitude on a scanner, although it is not an ideal parameter for measuring the acoustic output given the frequency-dependent behaviour of bubbles. It can be seen that the relationship is nonlinear, as linear behaviour would manifest itself as a horizontal line. Based on experimental results, an increase of approximately 50 per cent in the normalized echo signal power would be expected if the MI changes from 0.05 to 0.1. Therefore, in order to properly quantify and compare TICs obtained under different MIs, the measurements need to be calibrated with the curve shown in figure 3*b* experimentally obtained using a similar bubble population. However, the exact properties of the bubble population *in vivo*, including the size and coating properties, are difficult to measure and vary with time owing to factors discussed in §§3 and 4.

2.2. Focal depth

Changes to the focal depth of the scanner alter the spatial profile of the ultrasound beam. Consequently,

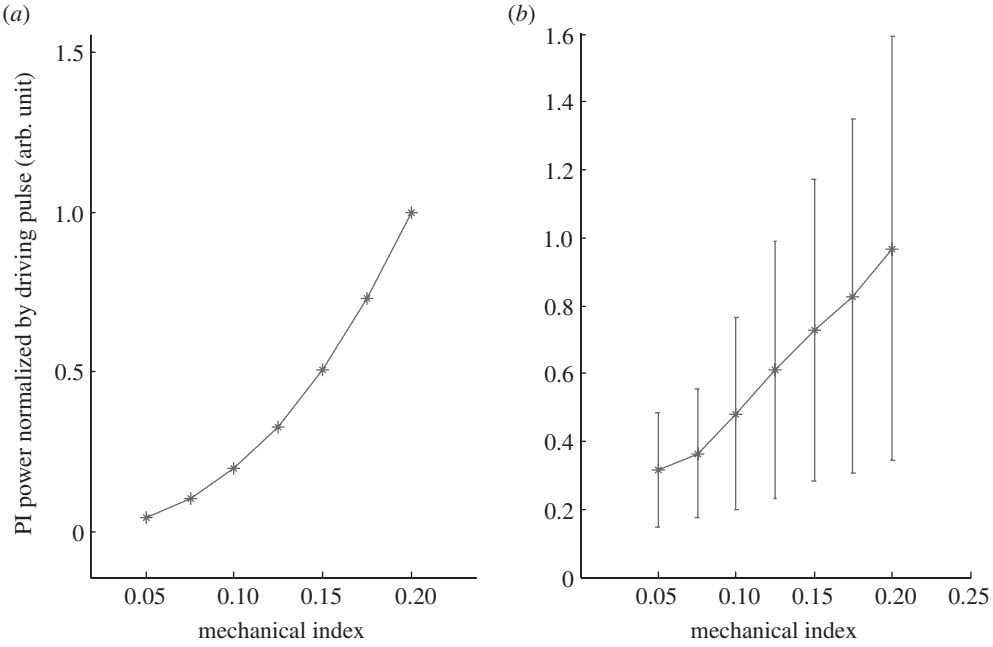

Figure 3. Pulse Inversion (PI) signal normalized by MI as a function of MI for SonoVue bubbles. (*a*) Simulation results (simulation settings follow those in Tang & Eckersley [32] and (*b*) experimental results. Experimental setup was similar to Tang & Eckersley [25]. Broadband pulses with a central frequency of 3.5 MHz were used. The experimental results show a quadrature relationship between PI signal and MI, while the simulation suggested higher orders. This is probably due to the bandwidth limit of the experiments where only second harmonics were retained in the PI signal, while in simulation higher order harmonics were also included. The large error bars in the experiments are probably due to the large variations of bubble population within the small focal volume of two transducers during each repeat and bubble destruction at higher MIs.

the ultrasound pressure amplitude becomes higher in some regions and lower in others. Although scanner manufacturers may adjust the driving voltage applied to the transducer when the focal depth is changed to ensure a constant MI at the focus as far as possible, an ROI may be exposed to different parts of the ultrasound beam and therefore bubbles in the ROI may be sonicated differently depending on the relative position of the ROI and the focal zone depth. Such changes in the spatial distribution of ultrasound amplitude as a result of focus change will probably affect TICs formed from dynamic CEUS image loops. Since bubble signals depend nonlinearly on ultrasound amplitude and the exact spatial distribution of tissue attenuation will be unknown, the effects of focus changes on images are complex.

A study by Koster *et al.* [23] reported significant influences of focal depth in harmonic power Doppler images. Changes of more than 100 per cent in the estimated flow index, β, were observed when the focal depth was changed from 7 to 17 cm. In a more recent series of indicator-dilution experiments developed with an *in vitro* flow phantom setup [33], the coefficient of variation for amplitude-related parameters (peak intensity and area under the curve (AUC)) was 33 and 36 per cent. By contrast, it was less than 6.3 per cent for time-related features (rise time and mean transit time). It was further observed in Gauthier's study that if the ROI is placed far from the focal depth, a change in the ROI position would have little impact on the measured features, especially those related to amplitude. These results may further justify the methodology used clinically in Averkiou *et al.* [34] whereby the focus was placed well below the target lesion to ensure a more uniform acoustic field.

To remove the effect of focal depth completely, the TICs need to be calibrated with two pieces of information: (i) the spatial pressure profiles of the ultrasound beam, and (ii) the bubbles' response to ultrasound amplitude (figure 3). To obtain the former, the spatial profile of tissue attenuation is required, which can only be estimated. The requirements for the latter are discussed subsequently. Further studies are needed to establish the feasibility of such methods.

2.3. Dynamic range and gain

Linearized log-compressed data are widely used to derive TICs for quantification as most clinical users do not have direct access to linear data [35–37]. Consequently, the quantification can be significantly affected by the dynamic range and gain settings. Linear data result from quadrature bandpass filtering of the digital radiofrequency data, which are then log-compressed according to propritetary formulae to reduce their dynamic range. Log-compressed data are finally converted to arbitrary unit data by application of a user-adjustable dynamic range (a.k.a. compression). In order to correctly reverse the logarithmic compression process, one may use either manufacturer-supplied software (e.g. Philips's QLAB, Toshiba's CHI-Q), or experimentally derive the linearization scheme with measurements from tissue phantoms. During this process, however, pixel intensities outside a limited dynamic range will not be correctly linearized. With non-destructive low-MI contrast imaging, the amplitude of the backscattered

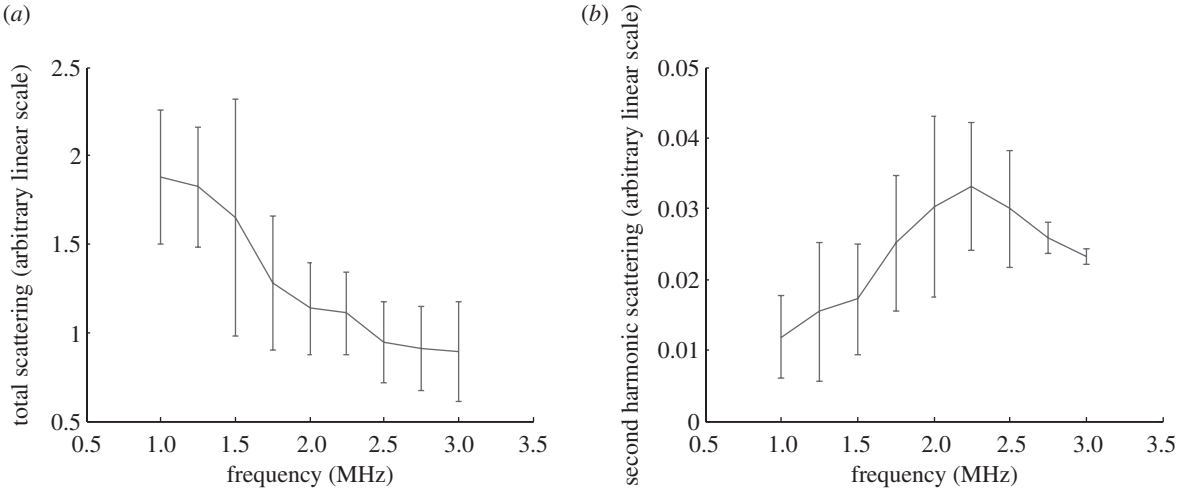

Figure 4. (*a*) Normalized total scattering power and (*b*) second harmonic scattering power as a function of driving ultrasound frequency. Experimental setup as described in Tang & Eckersley [25]. Briefly narrow-band pulses were transmitted through an acoustically transparent chamber containing Sonovue microbubbles (150 μl l^{-1}). The pulses have an MI of approximately 0.07 and a frequency ramp from 1 to 3 MHz with a step of 0.25 MHz. Two separate broadband focused transducers (Panametrics NDT Videoscan) were used as the transmitter and the receiver.

signals from bubbles is low; clinical ultrasound scanners therefore usually operate with a small dynamic range (typically between 10 and 30 dB as default) for better image presentation. This may lead to signal saturation and hence prevent proper linearization of the log-compressed data.

In a recent experimental and clinical study [36], the errors in the peak intensity and AUC derived from linearized log-compressed data, with linear data as references, were found to be $45 \pm 18\%$ and $39 \pm 16\%$, respectively, under a typical clinical dynamic range setting of 30 dB and a gain of 55 dB. By contrast, the error was found to be less than 5.4 per cent for all studied features (which included peak intensity and AUC, but also rise time and mean transit time), when a high dynamic range setting (at least 50 dB on the Philips scanner iU22) was used and the gain was carefully adjusted to ensure a high signal-to-noise ratio and to avoid signal saturation. Time-related parameters on the other hand were found to be much less affected.

2.4. Frequency

In order to achieve clinically useful spatial resolution, the transmitted pulses from the scanner must be broadband, and hence contain a range of frequencies. The central frequency of the pulses can be adjusted by the operator. It has been well demonstrated that bubble behaviour is highly dependent on the ultrasound frequency [1,38]. The unique resonance behaviour of the bubbles means that there is usually a peak in the scattering spectrum, although the amplitude and the frequency of this peak depend on the size and other properties of the contrast agents and their environment. Most previous studies that demonstrated such a peak only considered the overall scattered signal or scattering at the fundamental frequency [25,39–41]. For contrast-specific images, bubble scattering at higher harmonic or subharmonic frequencies is more relevant. Frinking & de Jong [42] have shown an approximate 4 dB (60%) change in second harmonic scattering for a simulation of Quantison when the driving frequency changes from 2 to 5 MHz. Sboros [43] showed a much higher change in second harmonic scattering for individual BiSphere bubbles when the driving frequency changes from 2 to 2.25 MHz. As a result, the absolute scale of a TIC may change significantly as frequency changes with a much lower image intensity expected at frequencies away from bubble resonance. Our experimental results (figure 4) show that at an MI ~ 0.07, a change of approximately 30 per cent in bubble second harmonic scattering signals can be expected when the transmit central frequency changes from 2.25 to 3 MHz. Furthermore, the frequency dependence for total scattering and harmonic scattering from the bubbles is very different.

The dependence of bubble signals on frequency means that in order to compare two TICs acquired at different ultrasound frequencies, the TICs need to be calibrated by the frequency response of the bubbles. It should be noted that attenuation of ultrasound is also frequency dependent and this will be further discussed in §3.4.

3. THE PATIENT

3.1. Blood pressure

The ambient pressure for bubbles is determined by the local blood pressure, which affects the signals from bubbles both by altering their equilibrium radius and also their stability. Blood pressure varies across a large range depending on the location (arterial, capillary or venous), the phase of a heart cycle and the condition of the patient. For example, typical systolic arterial blood pressure can vary between beats from 90 to 140 mm Hg (12.0–18.7 kPa) and between 60 and 90 mm Hg (8.0–12.0 kPa) in diastole across the population [44]. This cyclic variation modulates the bubble behaviour at the heart rate. The pressure could decrease to 10–30 mm Hg (1.3–4.0 kPa) in the

capillaries and to less than 1 mm Hg (0.13 kPa) in larger veins.

3.1.1. Effects on scattering/dynamics. The ambient pressure has a direct effect on the mean size and the resonant frequency of the bubbles, and hence the strength of the signals scattered from these bubbles. The past relevant literature has mainly focused on using this effect for non-invasive blood pressure measurements. An early study on this by Fairbank & Scully [45] reported that changes in the ambient pressure of the order of 0.2 atm (20 kPa) gave an observable shift in the resonant behaviour of gas bubbles of radii between 30 and 40 μm. Using a rabbit heart model, Moravi *et al.* [46] observed an approximately 20 per cent decrease in video intensity for albumin-coated bubbles during systole compared with diastole owing to the pressure difference. Shi [29] has compared scattered signals from Levovist, a galactose-based bubble, at different harmonic frequencies as a function of ambient pressure. The study reported a change of 10 dB for scattered subharmonic signals over the pressure range of 0–186 mm Hg (0–25 kPa), while at fundamental or second harmonic frequencies, the change was less than 3 dB. Similar results were also reported for Optison, Definity, Sonazoid and Levovist in Leodore *et al.* [47] and for SonoVue [48].

In summary, the effects of ambient pressure on imaging intensity can be significant, depending on the type and location of the vessels and the type of imaging mode. Given that the large variations in blood pressure are more likely to exist in large arteries, the effect can be reduced if ROIs are chosen to avoid such vessels.

3.1.2. Effects on diffusion/destruction. De Jong *et al.* [49] observed that albumin bubbles tend to shrink and disappear if a hydrostatic pressure of about 0.2 atm (20 kPa) is applied. This disappearance is attributed to passive dissolution. Shapiro *et al.* [50] observed similar effects. In Moravi *et al.* [46], an 8 per cent decrease in video intensity over 25 heart cycles owing to bubble destruction was observed. In Vuille *et al.* [51], Albunex bubbles were suspended in saline solution and imaged at 2.5 MHz; the rate at which contrast disappeared was greater at higher pressures by multiples of two, three and nine, respectively, for the 0.06, 0.13 and 0.19 atm (6, 13 and 19 kPa) measurements. Further, it was seen that the contrast reduction was an irreversible process. Gottlieb *et al.* [52] and Brayman *et al.* [53] reported similar observations.

Under conditions where blood pressure may be subject to local fluctuations, the effect may influence bubble persistence and in turn image intensity. For example, it has been found that left ventricular opacification can be significantly reduced in patients with reduced cardiac output caused by heart disease [54]. The specific cardiac conditions underlying the reduced output in the study included mitral and tricuspid regurgitation, atrial fibrillation, systolic dysfunction and pulmonary hypertension, perhaps suggesting that local spikes in blood pressure destroy the circulating bubbles, in turn reducing image contrast. However, it should also be considered that pressure may not be the sole mechanism for the effect, since high local shear forces may also be generated, which would also result in enhanced bubble destruction. Furthermore, it is not clear how much variation in heart rate would affect the bubble destruction and further study is needed.

3.2. Physiological interaction of the body with bubbles

Once injected into the human body, the interaction of circulating gas bubbles with the patient's physiological environment may also influence quantitative imaging. There are four dominant mechanisms widely acknowledged to be capable of influencing image intensity and transient contrast imaging: filtration of bubbles by the lungs, phagocytosis of bubbles by the reticular endothelial system (RES), recirculation of bubbles within the circulation and alteration of the local gas concentration gradient owing to inhaled anaesthetics. Each of these factors is discussed in more detail below; however, although each has received some attention from the research community, this has primarily been in the form of pharmacological characterization of the agents, while their effect on quantification is still barely understood. This section therefore comprises further explanation of the mechanisms involved, and discussion of the qualitative evaluation available.

3.2.1. Lung filtration. The influence of lung filtration on bubble size distribution and concentration is well recognized [49]. An early investigation using modelling to investigate the lack of detectable linear backscattering from bubbles in the myocardium concluded that the filtration of larger bubbles by the capillaries of the lung strongly influences the detected signal [41]. The effect has also been confirmed *in vivo* using intravital microscopy of rodent models to compare the effect of intravenous and intra-arterial injection of Definity bubbles. Following intra-arterial injection, used to model pulmonary filtration, large bubbles became trapped ($1.2 \pm 0.1\%$), while trapping was negligible owing to a lack of large bubbles following intravenous delivery, suggesting bubbles reaching the ROI had previously been subject to filtration in the lungs owing to their sizes [55]. It is likely that the effect of this filtration is to reduce bubble numbers, particularly the number of larger bubbles (greater than 10 μm in diameter), as illustrated in figure 5, while also lowering the overall bubble concentration. Consequently, the acoustic signal and dissolution kinetics of the bubbles that remain in circulation will be influenced.

In addition to filtration, the passage of bubbles through the lungs and exposure to blood at low pressure with a high oxygen and nitrogen concentration can cause diffusion of these gases into the bubbles as they pass through the pulmonary circulation [57]. While this gas will later diffuse out as local conditions within the systemic circulation change, the immediate effect will be to increase the number of large bubbles, which may in turn increase the influence of lung filtration.

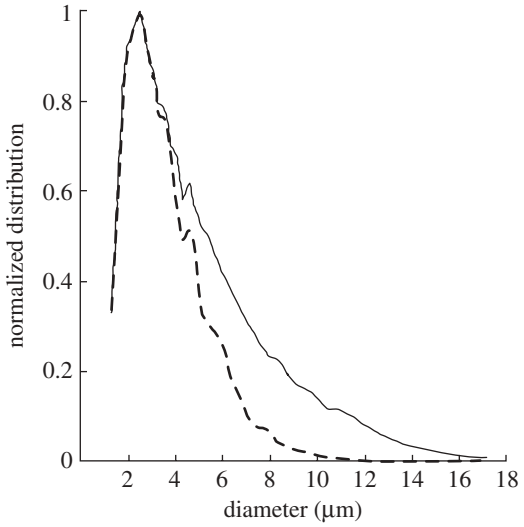

Figure 5. The size distribution of a native (solid line) and simulated lung filtered suspension (dashed line) of Albunex. Reprinted from [56] *Ultrasound Med. Biol.* v33, Bouakaz, A. & de Jong, N. WFUMB safety symposium on echo-contrast agents: nature and types of ultrasound contrast agents. 187–196, Copyright (2007), with permission from Elsevier.

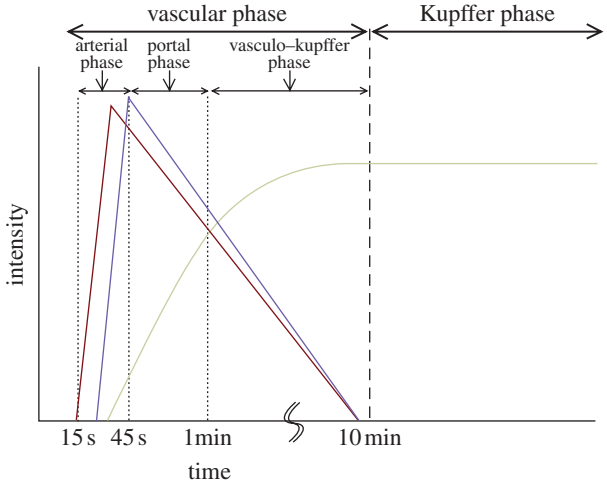

Figure 6. Identification of the vascular and Kupffer phases during liver contrast imaging using Sonazoid as proposed by Shunichi *et al.* [65]. Red, hepatic artery; blue, portal vein; green, parenchyma. Reprinted from [65] *Ultrasound Med. Biol.* v35, Shunichi, S., Hiroko, I., Fuminori, M. & Waki, H. Definition of contrast enhancement phases of the liver using a perfluoro-based microbubble agent, perflubutane microbubbles. 1819–1827, Copyright (2009), with permission from Elsevier.

Thus, the passage of bubbles through the lungs changes both bubble concentration and size and could introduce variations in quantification, especially when multiple doses are applied to the same patients when the physical and physiological conditions of the lung could have been altered by the previous injection. This is further discussed in §3.2.2 on possible phagocytosis of bubbles in the lung. Furthermore, lung filtering has important implications for the comparison of *in vivo* and *in vitro* experimental results [58].

3.2.2. Phagocytosis. A number of commercial contrast agents have demonstrated a 'late phase' in the parenchyma of the liver and spleen [59–61]. In general, this 'late phase' describes an enhancement in contrast that occurs more than 5 min after IV injection of the contrast agent. It has been suggested the effect may be attributed to slower bubble travel in the liver sinusoids [62] and the phagocytosis of certain contrast agent bubbles by the RES [63], with the macrophages of the liver (Kupffer cells) playing a dominant role in phagocytosis for Sonazoid and Optison [64]. The bubbles remain acoustically active even once phagocytosed for up to 2 h post-administration [65], strongly influencing the ultrasound signal intensity. As a result, late-phase imaging has been used to detect small hepatic malignancies [66], and alongside TIC measurements to provide a means of assessing the transient kinetics of the liver and therefore its associated pathology [67]. The association of the 'late-phase signal' with inflammation also offers the potential for imaging other disease states, such as atherosclerotic plaque inflammation [61].

A number of studies have indicated that the type of the contrast agent dictates the extent and duration of uptake [63,64,68]. Maruyama *et al.* [68] attempted to quantify the differences in the TIC generated by two contrast agents, Levovist and Definity, in rabbits. They revealed that while the signal intensity remained broadly similar over time in the portal vein for the two agents, there was a significant increase (up to four times greater) in the signal intensity for Levovist over Definity in the liver parenchyma. Yanagisawa *et al.* [64] performed a more comprehensive study of several contrast agents *in vitro* to determine that Sonozoid and Optison showed much greater uptake (99%) than Levovist (47%), SonoVue had the second lowest uptake (7.3%) and Imavist showed no uptake. In contrast to the other agents investigated, the uptake of SonoVue in this *in vitro* investigation was not sufficient to influence ultrasound image intensity at the concentrations employed. In another study, it was observed that irradiation owing to radiotherapy can significantly reduce the phagocytosis of Levovist microbubbles, probably owing to the damage to the Kupffer cells and the vascular endothelium [69].

The impact of bubble phagocytosis may extend beyond influencing the gradient of the TIC and impact on signal intensity. Bubbles that persist once phagocytized by Kupffer cells *in vitro* have been shown to respond differently under ultrasound insonation owing to oscillation damping when compared with those that remain outside the cells [70]. Using the same ultrasound parameters as a clinical study, bound bubbles were also found to be more stable under insonation than free bubbles. The impact of these phenomena on the quantitation of bubbles and how this relates to liver pathology need to be more fully understood. For example, while the time scales of the so-called vascular and Kupffer phases are established (figure 6) [65], quantification of the effect of tissue malignancy and inflammation, which will influence Kupffer cell density, on the latter phase has not been thoroughly investigated. Further, if a large proportion of the bubbles injected is retained in the liver, then this will alter the concentration of freely flowing bubbles elsewhere in the body and must be accounted for.

Finally, the effects of phagocytosis in the lung are thought to be involved in the increase in contrast

sometimes observed during a second contrast agent injection. Skrok [71] performed a quantitative investigation into the effect of a second injection on liver and aorta enhancement in healthy volunteers. The second injection, administered 12 min after the first and following complete disappearance of the enhancement showed a 5 ± 1.5 dB increase in peak intensity and the signal remained at least 3 dB greater than following the first injection for the remainder of the study. They hypothesized that the increase in intensity was caused by saturation of pulmonary macrophages by the first injection, leading to increased signals from the second.

3.2.3. Recirculation. Early research by Uchimoto *et al.* [72] suggested that the majority of Levovist bubbles circulate through the body's vasculature in the same way as red blood cells, without retention; thus, a bubble could circulate around the body in just less than a minute under normal resting conditions. Later this finding was confirmed for other contrast agents [55], and therefore the influence of bubble recirculation on any TIC measurements made using either bolus contrast agent administration or constant infusion should be considered. The effect of recirculation on the TIC would manifest itself as a small increase in contrast intensity approximately 60 s following the start of agent administration. However, the extent of the effect of recirculation remains difficult to quantify. One confounding factor is the gradual spatial spreading of the contrast agents within the vessels over time. In case of a bolus injection, while recirculation is likely to influence the tail of the TIC [34], the change is likely to be smooth and gradual and hence difficult to identify because the bolus profile would in any case gradually spread out becoming 'wider' and 'flatter' after the initial circulation. A similar phenomenon exists in the case of constant infusion of contrast agents, except that spatial spreading only occurs at the front of the infusion profile, potentially causing fewer problems. Furthermore, for constant infusion with destruction and reperfusion, the time scale of the reperfusion is usually short and the recirculation of bubbles would not affect the shape of the TICs to a great extent but rather add a constant bias. The effects of recirculation are further confounded by the gradual decay of bubbles over time, which is discussed in §4.1.2. In terms of the relative significance of the recirculated bubbles, further studies are needed to compare the concentration of the recirculated bubbles with that at the tail of the initial bolus in the case of a bolus injection, or with that of the newly infused bubbles in the case of a constant infusion.

To address the problems associated with recirculation, some researchers have considered for bolus injection only the wash-in phase of the curve [33,34], or limited the time window post-injection during which scanning takes place [66].

3.2.4. Anaesthetics. The administration of anaesthetics during contrast imaging can influence the TIC in two ways, firstly through the pharmacological effects of the anaesthetic itself and secondly, in the specific case of inhalation anaesthetics, through the influence of the inhaled gases on local blood gas concentration and hence on gas diffusion between bubbles and the environment. In the latter, alterations in the local blood gas concentration caused by the anaesthetic or co-administered gases, such as air or oxygen, will alter the size distribution and therefore the echogenicity of the contrast agent suspension, a dominant factor influencing quantitative measurements. Mullin *et al.* [73] looked at the effect of changing the carrier gas used during isoflurane anaesthetic administration in rats and found medical air improved bubble stability by 3.3 ± 1.5 times when compared with pure oxygen during imaging. The influence of local gas concentration on bubble behaviour and on the TICs is discussed in more detail in §4.4.

Several investigators have identified the pharmacological effect of vasodilation in association with anaesthetic use [74–76]. Nyman *et al.* [76] investigated the influence of the IV-administered anaesthetic Propofol on ultrasound contrast imaging of dogs; those treated with the anaesthetic demonstrated a faster time to peak intensity (46.3 s) than those without anaesthetic (34.6 s), with the difference attributed to the vasodilator effect of the anaesthetic used. Vasodilation will alter local blood pressure and heart rate, each factors identified in previous sections as influencing quantitative imaging. As above, the effect is also commonly associated with, though not restricted to, the use of inhaled anaesthetics [74,75], making it particularly relevant to *in vivo* animal studies where inhaled anaesthetics are widely used.

3.3. Tissue motion

A TIC is extracted from a time series of images by taking the pixel intensity or the averaged pixel intensity of the corresponding regions from every image in the series. This requires correction for any tissue movement during the acquisition so that spatial correspondence for pixels or regions between image frames can be properly established. Tissue movement can be caused by a pumping heart or patient breathing. Effects of such movements on the TIC can be seen in figures 2 and 7, where the signal oscillations were mainly caused by tissue motion. The amplitude of variation strongly depends on what kind of features move in and out of the ROI. For example, a large vessel full of bubbles moving in and out of the ROI could cause intensity variations of hundreds of per cents.

Various motion correction algorithms are available that can deal with translation, rotation or non-rigid deformation of tissues. While most quantification packages have already incorporated such algorithms, they are only able to deal with in-plane motion. Out–of-plane motion means different tissues are imaged at different times, and this type of motion is impossible to correct for with scans on only a single plane. One way to deal with this is to track the motion and only use a subset of the image sequence that corresponds to the same anatomical cross section. This can be done either by using ECG gating for cardiac motion, or by identifying some anatomical landmark(s) within

the images as a marker of a certain anatomical cross section since out-of-plane motion can cause the landmarks to disappear in the image [34]. However, such methods have drawbacks. For example, they reduce the number of imaging frames that can be used; the landmarks may not always be available. To completely solve this problem, image acquisition and registration needs to be done in three dimensions (or four dimensions if time is counted as another dimension). In addition, it has been shown in the quantification of perfusion in the kidney that comparing with two dimensions, imaging and quantification in three dimensions can significantly reduce the variations for an inhomogeneous perfusion volume [77].

3.4. Tissue attenuation

TIC measurements for a specific ROI are directly influenced by the attenuation properties of the medium the acoustic wave traverses to reach it. For example, two regions containing similar bubbles may have a different peak and shape of the TIC owing to differences in the propagation path. Leinonen [78] has reported a significant decrease in the peak intensity of the TIC as the depth (as well as the size) of the ROI increases. Attenuation properties for human tissues have been well studied in the past and reference values are available [79], but values vary significantly with tissue type and across the population, and may also be influenced by pathology [80]. The presence of bubbles adds further to the attenuation [81,82], with the extent dependent on the bubble concentration within the organ of interest and the tissues preceding it. In the cardiac chambers, for example, attenuation can be up to 10–20× greater than within the soft tissues [83]. Similarly in the liver, where blood constitutes approximately one-third of the volume, bubbles may contribute significantly to the attenuation. The attenuation by both tissue and bubbles are frequency dependent. While tissue attenuation increases with frequency, bubbles attenuate most at the resonance frequency.

If not properly compensated for, attenuation can cause large variations in signal intensity and therefore influence the peak of the TIC. Although timing indices such as peak time are generally less affected by attenuation (and other factors affecting intensity), time-varying attenuation owing to the passage of excessive amount of bubbles in the overlaying tissue could alter the shape of the TIC and affect the timing indices as well [81]. It should be noted that owing to the logarithm compression of the ultrasound images, significant variations in TIC could still exist even when two regions visually appear similar. Such an example is shown in figure 7.

In clinical ultrasound scanners, the attenuation is partly compensated for through the adjustable time gain compensation (TGC) control. Yano *et al.* [84] reported that attenuation as high as 15.8 dB (approx. 40 times) within parts of a normal myocardium could be corrected through an image calibration technique to an average of 6.3 dB. However, the manual method proposed was labour intensive and required an experienced operator. In most clinical imaging systems, such adjustments can be made manually but this introduces additional operator-dependent variations and can make it difficult to handle changes in attenuation in real time. Existing automatic TGC functions on the other hand are limited in their applicability to quantification since they are optimized for visualization rather than quantification, and no clinical imaging system currently implements compensation that accounts for the unique nonlinear attenuation generated by bubbles.

The attenuation owing to bubbles is known to be nonlinear with respect to ultrasound amplitude [25,26,85]. Recently, a number of promising algorithms specifically designed for correcting attenuation in contrast-specific ultrasound images have been reported [82,86–89], and the value of these attenuation correction algorithms in clinical applications needs to be further validated.

3.5. Nonlinear propagation

3.5.1. Nonlinear tissue propagation. Another factor influencing the TIC for a given ROI is the nonlinearity of the overlaying tissue. As the pulse propagates through tissue, it can be distorted and part of the pulse power is transferred from the fundamental transmitting frequency to higher harmonics. However, nonlinear propagation in tissue without contrast enhancement has been shown to be insignificant at the relatively low MIs (less than 0.1) typically used clinically [90].

3.5.2. Nonlinear bubble propagation. It has been shown that even at an MI as low as 0.05, which is almost the lowest MI achievable in a clinical scanner, significant nonlinear propagation can occur within a bubble cloud of a relatively low concentration [90]. This has been shown to cause two types of imaging artefacts [32]. Firstly, tissue is misclassified as bubbles and secondly, bubble concentration is misrepresented. While the former type seems to be the most important and has been reported both with laboratory phantoms [32,90,91] and clinically [92] and could lead to misdiagnosis, the latter type could also become significant when the driving frequency is away from the resonance frequency of the bubble population, e.g. in high-frequency imaging where only a small proportion of the population undergo nonlinear oscillation. A clinical example of the former type of artefacts owing to nonlinear propagation is shown in figure 8.

A few recent papers have been dedicated to the development of nonlinear artefact correction methods [93–95]. These methods all use driving signals containing harmonic components so that these signals will cancel those generated by nonlinear propagation. However, these methods are only effective locally within a certain depth range and could cause additional artefacts elsewhere in the image. On the other hand, models for nonlinear propagation through a bubble population could lead to a model-based strategy to correct the nonlinear artefacts. However, existing models do not agree well with experimental data and their implementation can be computationally expensive

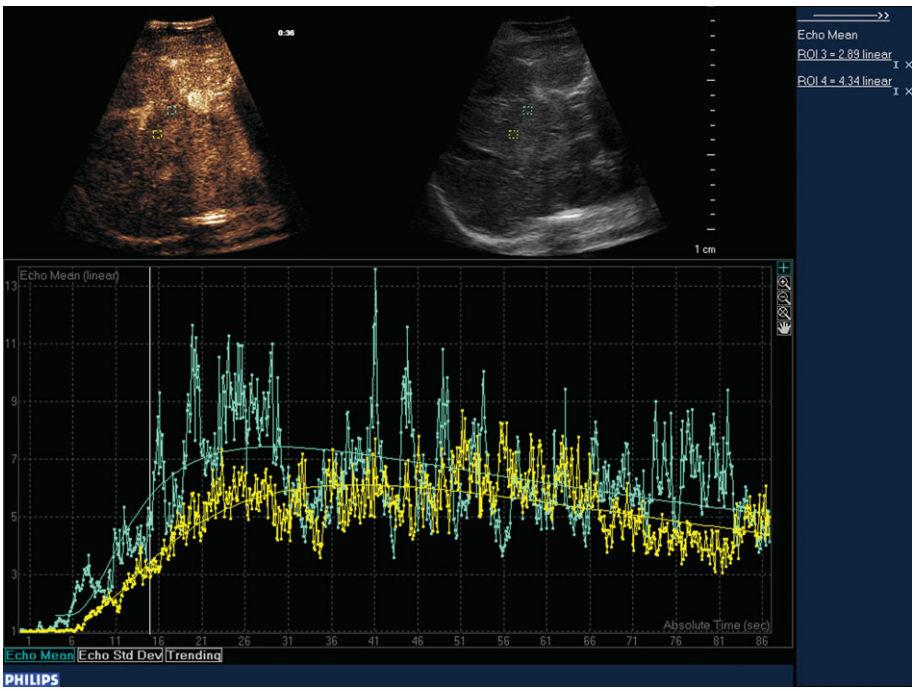

Figure 7. A contrast-specific image of a human liver (top left image), the corresponding B-mode image (top right image) and the TICs for two ROIs (bottom graph). The two ROIs are from similar tissue type and appear similar in the images, but their TICs are actually different owing to acoustic attenuation and other factors.

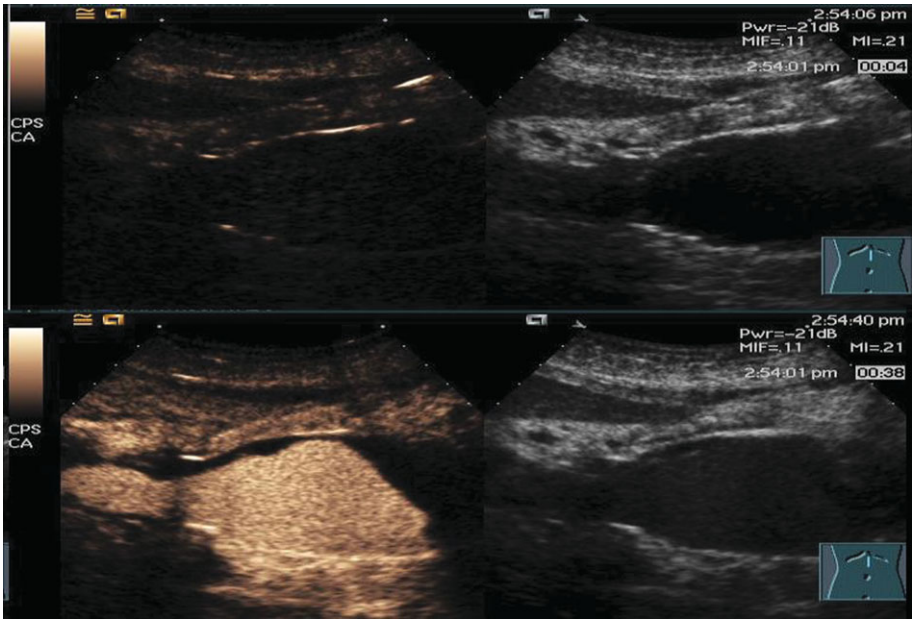

Figure 8. Cross section of an aorta on contrast-specific images (left images) and traditional B-mode images (right images) and before contrast enhancement (top images) and after (bottom images). Nonlinear artefacts (indicated by the solid arrow) are clearly visible on the lower right area of the bottom left image.

[32,96]. These issues are further addressed in some recent studies [97,98].

4. BUBBLES AND HANDLING

4.1. Bubble type

As discussed in §1, there are a number of different bubble agents available for clinical use (table 1) and an even greater number under development for research purposes. These agents differ both in terms of their composition and size distribution, which are the key properties determining their behaviour *in vivo* and hence their acoustic properties for perfusion studies. Most important is the effect of the bubbles on the scattering and attenuation of ultrasound in the tissue in the ROI, but transit properties, such as arrival time within an organ [99] filtering to produce subpopulations [100] and persistence will also influence perfusion measurements. The physical

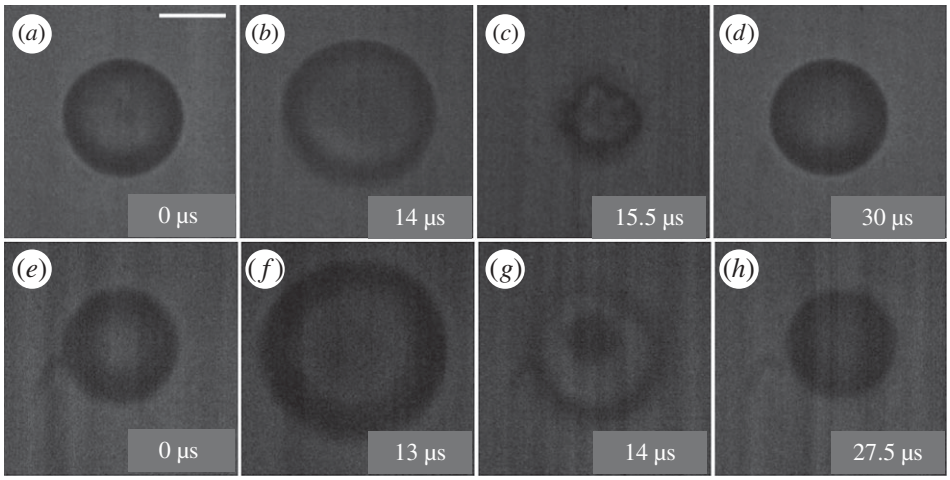

Figure 9. Still images taken from high-speed imaging acquisitions of two SonoVue bubbles of similar initial diameter (approx. 9.2 µm) excited at 100 kPa, 0.5 MHz. The images illustrate the differences in oscillation observed between bubble 1 (*a*–*d*) and bubble 2 (*e*–*h*), where (*a*,*e*) and (*d*,*h*) show the initial and end diameters of each bubble, and (*b*,*f*) show the maximum radial expansion for each bubble. Note the shell crumpling observed in bubble 1 only (*c*), and the jetting observed in bubble 2 only (*g*). High-speed imaging was performed using a Cordin 550 at two million frames per second. Scale bar is 5 µm.

characteristics of the bubbles will also determine the extent to which they are influenced by conditions *in vivo*, which may further influence their acoustic response. The significance of each of these factors requires careful consideration for the further development of quantitative imaging techniques.

4.1.1. Bubble size and coating. The key requirement for quantitative imaging is the accurate definition of the relationship between measured backscattered ultrasound intensity and the population of bubbles within the ROI. An essential step is therefore to establish the bubble size distribution, e.g. through a Coulter counter [101] or under a microscope [102], since this is the main determinant of the acoustic response [103]. Currently, all the commercial agents have broad size distributions and the mean size differs significantly between agents, making comparison of quantification using different agents difficult. Even for the same agent, the way it is reconstituted prior to administration may introduce significant variations in both size and concentration owing to, e.g. manual shaking of vials. Such variations during reconstitution, together with further variations caused by administration and the physical and physiological conditions in the immediate environment (cf. §3), means the size distribution of commercial agents provided by the manufacturers does not provide a sufficiently accurate indication of the bubble size distribution *in vivo*.

The bubble coating is a further important factor determining the acoustic response [91]. Its effective mechanical properties, which are typically characterized in terms of an elastic and viscous resistance, determine the bubble resonance frequency, amplitude and linearity of oscillation. Studies of Albunex, an air-filled forerunner of Optison, show that the stiffer albumin shell limits its response to ultrasound when compared with the lipid-shelled agent Definity [104,105]. Similar results are also reported in a comparison between Levovist and Definity [106]. Accurate, repeatable characterization of coating properties has yet to be demonstrated, however, and the existing data indicate that there is a considerable degree of variability within a given bubble population [107]; figure 9 shows significantly different behaviour of two Sonovue bubbles of a similar initial diameter, indicating significant difference in their coating. This represents a further source of uncertainty in the interpretation of the backscattered signal.

In addition to the mechanical properties of the bubble shell, its characteristics can also influence biological interaction. Fisher *et al.* [108] demonstrated that the surface charge of the bubble shell can influence passage through the circulation and retention, and most lipid-shelled bubble contrast agents include a polyethylene glycol component to improve biocompatibility, reduce detection by the RES and prevent coagulation. The commercial contrast agents currently available are the result of a considerable and on-going body of work relating to the optimization of shell materials and additives. Several research groups have contributed to this body of knowledge [109–112].

4.1.2. Stability and time-dependent behaviour. The initial bubble size distribution and concentration will be affected by the handling and administration of the contrast agent as described in §4.2. Once injected, these will also be subject to change, as will the properties of the bubble coating. The relationship between the backscattered signal and bubble population will thus be a function of time, which may in turn make it difficult to compare images acquired at different times. Figure 10 shows an example of a simple attenuation measurement for a gently stirred Sonovue suspension measured over 30 min *in vitro*.

Over relatively long time scales (minutes), the change in the bubble signal may be related to diffusion of the encapsulated gas into the surroundings. The first contrast agents (e.g. Albunex, Levovist) contained air and were relatively short-lived *in vivo*. Current

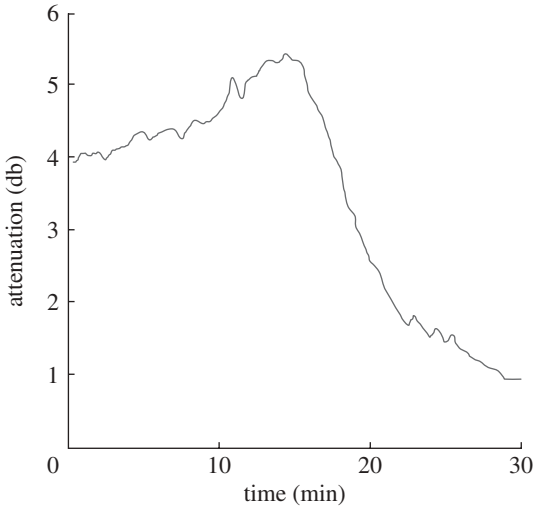

Figure 10. Attenuation measurements of a Sonovue suspension measured over 30 min in a gently stirred acoustic transparent chamber.

commercially available agents use higher molecular weight gases such as perfluorocarbons (cf. table 1) that diffuse more slowly while having a negligible effect upon the acoustic response. Modelling has been used to show that Optison actually expands owing to adsorption of air from the surrounding liquid until a concentration balance is achieved, following which the bubble dissolves [113]. The presence of the bubble coating provides a barrier to gas diffusion and reduces the interfacial tension at the bubble surface. Bubble stability is thus improved if the shell has a low gas diffusivity coefficient, and the gas core a low saturation constant and high density [114]. Numerous studies suggest the improved stability of lipid-shelled agents, through better prevention of gas dissolution, over those with a protein shell [100,105,115,116].

Recent studies have demonstrated that changes in bubble population are strongly correlated with the environmental conditions, specifically pressure, temperature and dissolved gas concentration [117]. Laboratory characterization should therefore be performed under conditions as close to those encountered *in vivo* as possible. Moreover, as discussed in §3, biological interactions may also produce significant changes in the bubble population. Changes in the bubble coating may occur both on the same time scale as gas diffusion, and also on the time scale of the acoustic pulse. In the case of lipid-coated bubbles, the latter is thought to be related to 'pinching off' or shedding of surplus coating material and effect has been demonstrated for both undriven [112] and driven bubbles [110]. For protein-coated bubbles, studies of Optison destruction indicate shell fragmentation occurs, followed by rapid dissolution of the now unencapsulated gas. Similar results have also been shown for polymer-coated bubbles [118]. The extent to which bubble destruction occurs will clearly depend upon the intensity of the ultrasound field and duration of exposure, with frequencies close to the bubble resonance and high intensities producing more rapid changes in the population.

4.2. Injection and handling

The methods used during the injection and handling of bubbles have been demonstrated to influence their physical properties, and this could influence their acoustic behaviour during quantitative imaging. The influence of repeated administration of the contrast agent on image intensity is addressed in §3.2.2, while this section focuses on the influence of injection and handling on a single dose of bubbles. Contrast agent suspensions come in a variety of different storage formats and require reconstitution through manual shaking (e.g. SonoVue; Sonazoid), reconstitution using a shaker (Definity/Luminity) or resuspension (e.g. Optison), as directed by the manufacturer, immediately prior to use. Once prepared, the size distribution, stability and concentration of the suspension can be influenced by several factors.

Contrast agent suspensions are normally used within between 30 min (e.g. Optison) and a few hours (e.g. Sonovue) of preparation with storage following activation leading to degradation and both loss of concentration and alteration of the size distribution. The effect can be exacerbated if the bubbles are kept in a heated environment, since raising the temperature above room temperature is known to influence the bubble stability and size distribution [117] as above. Bubble buoyancy means that suspensions must be re-suspended to ensure homogeneity immediately prior to use, and their susceptibility to local changes in pressure [119] means that vials should be vented using a sterile open needle or a pressure-controlling device (e.g. a MiniSpike in the case of Sonovue) during withdrawal to prevent destruction. The scale of the variations in contrast signals for sequential scans using the same agent vial has not been reported.

The diameter of the needle or the catheter and the method used for delivery (infusion or bolus) are likely to introduce potentially large errors in the administration of ultrasound contrast agents. Recent *in vitro* studies investigating the influence of the needle gauge on delivered bubbles found that reducing the needle inner diameter produced a large reduction in bubble concentration, as much as 99.9 per cent for needle diameters of less than 0.24 mm (less than 25 g) [120,121]. Recent work within our own group found that in addition to the needle gauge, needle orientation and the time taken to administer the contrast agent had a significant impact on bubble size and concentration *in vitro* and *in vivo* [122]. To replicate bubble administration *in vivo*, bubbles were withdrawn into a syringe, which was held vertically for 20 s to allow air bubble removal, and then horizontally for 20 s to simulate needle positioning for intravenous injection before the suspension was expelled for analysis. Delivery with a 29 g rather than a 25 g needle resulted in a reduction in the bubble delivered of over 30 per cent and 9 per cent reduction in mean bubble diameter. The effect of needle gauge is most relevant in pre-clinical investigations using small animals, where small gauge needles and catheters are required. However, the effects of needle orientation will impact both pre-clinical and clinical administration alike.

Further, for bolus injections, the injection rate and the dose of bubble suspension delivered are most likely to significantly influence the accuracy of quantitative imaging. An investigation comparing two injection rates in mice indicated that the faster the injection rate, the greater the peak magnitude for TIC, and faster the time to peak for TIC and maximum intensity over time [123], as illustrated in figure 11. For constant infusion, a recent investigation of the influence of infusion rate on perfusion estimates in rats revealed that low bubble concentrations (which in this case occurred as a result of a low infusion rate but may equally apply to bolus administration) resulted in a greater measurement bias, but this could be overcome by increasing the infusion rate [77]. However, the study was conducted using rats, so specific infusion rates for use in humans were not established. So far, to the authors' knowledge, there has been no report of a direct experimental comparison between bolus injection and constant infusion in terms of variations in quantification. In theory, constant infusion studies would be expected to suffer from less variability, since the contrast agent is commonly administered by an infusion pump in this case while bolus injections are commonly administered manually. This hypothesis does however require substantiating with clinical data.

Finally, although not common in clinical practice, dilution of the bubble suspension prior to injection is common in laboratory experiments, either in saline or for co-injection purposes. This may alter the gas concentration of the suspending fluid and therefore the size distribution and stability of the bubbles [124–126].

4.3. Dosage

The use of bubbles for quantitative imaging relies on the assumption that there is a linear (i.e. directly proportional) relationship between echo signal intensity and bubble concentration. A number of studies have demonstrated such a linear relationship [39,40] at relatively low doses. However, at high doses, two phenomena will affect this relationship: multiple scattering and attenuation.

The dynamic interactions that occur between ultrasound and bubbles can give rise to an effect known as multiple scattering, whereby the sound waves scattered by one bubble will affect the oscillation and hence scattering from its neighbours. This will alter the echoes obtained from highly concentrated bubble populations and make the relationship between concentration and signal intensity nonlinear. The effect is dependent on the number of bubbles that are acoustically active in the sound field [127], and therefore the effect is particularly relevant at high bubble concentrations and at high mechanical indices. *In vivo*, assuming uniform distribution throughout the circulation, concentrations of approximately 10^4–10^5 bubbles ml^{-1} would be expected, for which it is justifiable to neglect multiple scattering. When a contrast agent is injected as a bolus, however, the validity of this assumption has not been verified.

In addition, attenuation owing to high concentrations of bubbles can reduce the signal intensity produced from bubbles deeper within the image plane. In the absence of a proper attenuation correction technique, this can also cause a nonlinear relationship between concentration and signal intensity.

In a recent paper, Lampaskis & Averkiou [128] used a flow phantom to study the relationship between the clinically relevant contrast agent dose and image intensity for the contrast agent SonoVue. The relationship remained linear from 0.004 to 1 per cent in gas volume fraction, before becoming nonlinear and finally reaching a plateau at around 2 per cent. The study was conducted at a low MI (0.05) using a clinical scanner (iU22, Phillips Medical Systems) and the saturation attributed to attenuation and signal limiting owing to the gain and compression settings of the imaging system.

4.4. Gas concentration effects

The diameter and stability of bubbles within the circulation are strongly influenced by the dissolved gas content of the fluid that surrounds them [126,129]. The use of higher density gases, e.g. perfluorocarbon gasses, as used in most commercial preparations, is intended to retard the effect of gas transfer between the bubble core and the environment. However, while this has been demonstrated to improve persistence, bubbles remain highly vulnerable to variations in the gas saturation of the surrounding fluid. *In vivo*, the concentration of gases within the blood plasma generally remains approximately constant; however, oxygen saturation varies greatly around the body-generating conditions for both bubble expansion owing to gas influx (and low blood pressure) in the pulmonary circulation, and contraction owing to gas escape in the peripheral circulation. These effects are further influenced by the solubility of the stabilizing shell material and will therefore vary with the agent. Nevertheless, for a particular contrast agent, the influence of gas saturation, in the absence of any mitigating circumstances (e.g. inhaled anaesthetics, alterations to blood pressure), will remain approximately similar during each administration *in vivo*, while the effect of gas saturation during *in vitro* investigation can introduce considerable variability and should be carefully controlled.

5. CONCLUDING REMARKS AND FUTURE DEVELOPMENT

Exciting advances have been made in CEUS imaging in the past two decades, particularly in developing better agents, understanding the complex interaction between the agents, the ultrasound and the *in vivo* environment, developing techniques to generate images of remarkable quality and demonstrating a wide and continuously expanding range of clinical applications that could benefit from this technique. As a unique means of visualizing and quantifying vascularity and tissue perfusion, CEUS offers many significant advantages over existing imaging modalities such as CT and MRI. However, the clinical value of this technique is compromised by the relatively large variations in the imaging and quantification results. It is of crucial importance that this issue is addressed

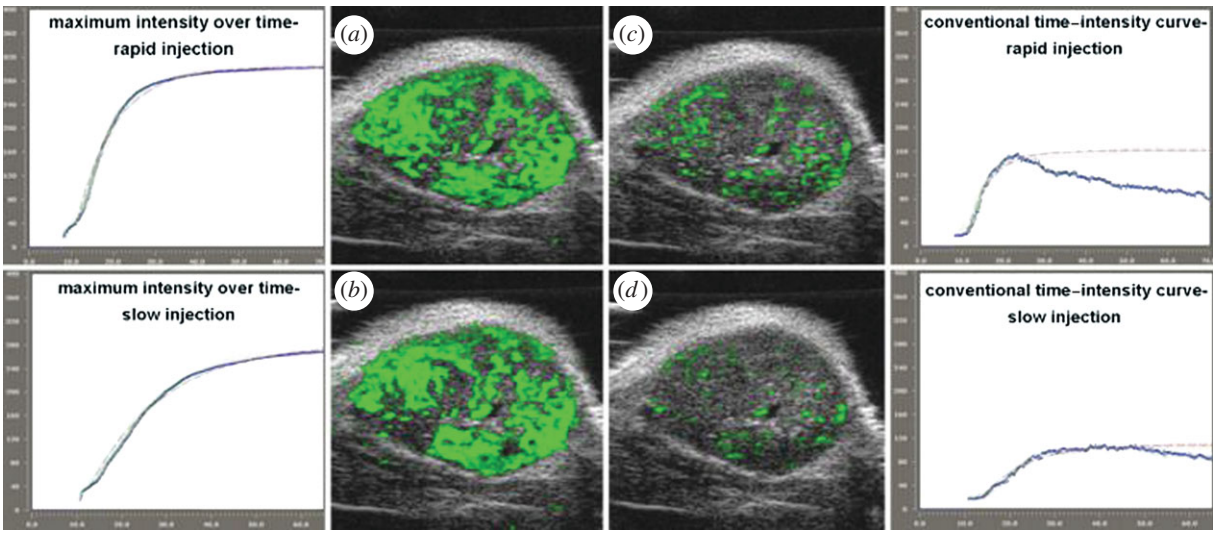

Figure 11. Influence of injection rate on the maximum intensity over time (MIOT) (*a*,*b*) and TIC (*c*,*d*) for two injection rates: 50 µl over 2 s (*a*,*c*) and 50 µl over 10 s (*b*,*d*) [123]. Note, the flow rates used relate to 1.5 and 0.3 ml min^{-1}, respectively. Reprinted from [123] *Eur. J. Radiol.* V75, Socher, M., Hauff, P., Bzyl, J., Semmler, W., Günther, R. W. & Kiessling, F. Comparison of conventional time-intensity curves vs. maximum intensity over time for post-processing of dynamic contrast-enhanced ultrasound. e149–e153, Copyright (2010), with permission from Elsevier.

in order for CEUS to be widely accepted clinically as a first-line imaging technique.

In this review, we have examined a wide range of factors that could contribute to the variations in contrast image intensity, including scanner settings, patient factors and bubble properties and handling. Factors in each of these categories can cause large variations in quantification results. Some potential ways of reducing the variation for individual factors have already been discussed, but to fully address this problem, a systematic approach is needed to tackle these factors.

Some empirically based methods have already been reported to reduce variations in quantitative contrast ultrasound. One is to standardize the data acquisition and processing protocols [130,131]. Such protocols include, e.g. fixing all scanner parameters and always using the same operator/procedure for bubble handling etc. [17]. Although these measures can effectively reduce the variations to a certain extent, they cannot deal with those caused by physiological or pathological variations of the patients. For example, if one patient has a more attenuating liver, a different acoustic window, a higher blood pressure or a lesion of interest deeper in the body than another patient, fixing the scanner settings would not be able to reduce the inter-patent variations. The other method to remove unwanted variations from non-local sources is the normalization of areas of interest (e.g. cancer) with neighbouring normal tissue as reference. Ideally, if the neighbouring areas are chosen to be close enough to the ROI, confounding factors such as attenuation, acoustic field geometry, the way bubbles are injected and handled and non-local patient factors that affect both the target area and the reference area could potentially be reduced or even removed. The normalization results become a ratio of the bubble concentration between the ROI and the reference region. However, this approach is significantly affected by operator expertise in choosing the reference regions, and this manual procedure itself introduces additional variations to the results. For example, the results would be very different if the reference region contains relatively large vessels or contains abnormal tissue.

Currently, imaging and quantification of bubbles are complicated by the fact that bubbles injected in the body have a wide range of distributions in terms of size and coating parameters, which are largely unknown. They also change over time owing to the factors discussed in this paper. This is further complicated by the fact that bubbles with different properties may change in different ways. New developments in the fabrication processes to generate more controlled bubble properties could open up new ways of addressing many of the issues. So far, significant efforts have been made to manufacture bubbles with a very high degree of control over bubble uniformity in terms of their size and coating properties [132–134]. This would potentially help the accurate prediction of the acoustic response of a bubble population exposed to ultrasound given specific scanner settings. Furthermore, these bubbles could be better suited for the measurement of *in vivo* environmental variables such as blood pressure, and hence lead to ways to reduce or remove their effects on quantification.

In the past two decades, the advances in the clinical applications of CEUS have been powered by advances in basic understanding of microbubble physics and technological developments, in particular in the areas of ultrasound system and transducer design and signal processing. This will certainly continue to be the case in the future. Through the deepening of our understanding of the sources of variations in quantitative CEUS, and the development and application of techniques to address them, the clinical application of CEUS will undoubtedly go far beyond what has already been achieved.

The authors would like to acknowledge the financial support from UK EPSRC (grant nos EP/G038163/1 and EP/F066740/1), the Royal Society and the Bagrit foundation.

REFERENCES

1 Becher, H. & Burns, P. N. 2000 *Handbook of contrast echocardiography*, 1st edn. Berlin, Germany: Springer.
2 Cosgrove, D. & Lassau, N. 2010 Imaging of perfusion using ultrasound. *Eur. J. Nucl. Med. Mol. Imaging* **37**, S65–S85. (doi:10.1007/s00259-010-1537-7)
3 Wilson, S. R. & Burns, P. N. 2010 Microbubble-enhanced US in body imaging: what role? *Radiology* **257**, 24–39. (doi:10.1148/radiol.10091210)
4 Sboros, V. & Tang, M. X. 2010 The assessment of microvascular flow and tissue perfusion using ultrasound imaging. *Proc. Inst. Mech. Eng. Part H J. Eng. Med.* **224**, 273–290. (doi:10.1243/09544119JEIM621)
5 Gramiak, R. & Shah, P. M. 1968 Echocardiography of the aortic root. *Invest. Radiol.* **3**, 356–366. (doi:10.1097/00004424-196809000-00011)
6 Kremkau, F. W., Gramiak, R., Carstens, E. l., Shah, P. M. & Kramer, D. H. 1970 Ultrasonic detection of cavitation at catheter tips. *Am. J. Roentgenol. Radium Ther. Nucl. Med.* **110**, 177–183.
7 Eckersley, R. J., Chin, C. T. & Burns, P. N. 2005 Optimising phase and amplitude modulation schemes for imaging microbubble contrast agents at low acoustic power. *Ultrasound Med. Biol.* **31**, 213–219. (doi:10.1016/j.ultrasmedbio.2004.10.004)
8 Wei, K., Jayaweera, A. R., Firoozan, S., Linka, A., Skyba, D. M. & Kaul, S. 1998 Quantification of myocardial blood flow with ultrasound-induced destruction of microbubbles administered as a constant venous infusion. *Circulation* **97**, 473–483.
9 Lindner, J. R., Villanueva, F. S., Dent, J. M., Wei, K., Sklenar, J. & Kaul, S. 2000 Assessment of resting perfusion with myocardial contrast echocardiography: theoretical and practical considerations. *Am. Heart J.* **139**, 231–240.
10 Strouthos, C., Lampaskis, M., Sboros, V., McNeilly, A. & Averkiou, M. 2010 Indicator dilution models for the quantification of microvascular blood flow with bolus administration of ultrasound contrast agents. *IEEE Trans. Ultrason. Ferroelectr. Freq. Control* **57**, 1296–1310. (doi:10.1109/TUFFC.2010.1550)
11 Hudson, J. M., Karshafian, R. & Burns, P. N. 2009 Quantification of flow using ultrasound and microbubbles: a disruption replenishment model based on physical principles. *Ultrasound Med. Biol.* **35**, 2007–2020. (doi:10.1016/j.ultrasmedbio.2009.06.1102)
12 Arditi, M., Frinking, P. J. A., Zhou, X. & Rognin, N. G. 2006 A new formalism for the quantification of tissue perfusion by the destruct ion-replenishment method in contrast ultrasound Imaging. *IEEE Trans. Ultrason. Ferroelectr. Freq. Control* **53**, 1118–1129. (doi:10.1109/TUFFC.2006.1642510)
13 Sugimoto, K., Moriyasu, F., Kamiyama, N., Metoki, R. & Iijima, H. 2007 Parametric imaging of contrast ultrasound for the evaluation of neovascularization in liver tumors. *Hepatol. Res.* **37**, 464–472. (doi:10.1111/j.1872-034X.2007.00060.x)
14 Rognin, N. G., Arditi, M., Mercier, L., Frinking, P. J. A., Schneider, M., Perrenoud, G., Anaye, A., Meuwly, J.-Y. & Tranquart, F. 2010 Parametric imaging for characterizing focal liver lesions in contrast-enhanced ultrasound. *IEEE Trans. Ultrason. Ferroelectr. Freq. Control* **57**, 2503–2511. (doi:10.1109/TUFFC.2010.1716)
15 Porter, T. R. & Xie, F. 2010 Myocardial perfusion imaging with contrast ultrasound. *Jacc Cardiovasc. Imaging* **3**, 176–187. (doi:10.1016/j.jcmg.2009.09.024)
16 Lavisse, S. *et al.* 2008 Early quantitative evaluation of a tumor vasculature disruptive agent AVE8062 using dynamic contrast-enhanced ultrasonography. *Invest. Radiol.* **43**, 100–111. (doi:10.1097/RLI.0b013e3181577cfc)
17 Lassau, N., Koscielny, S., Chami, L., Chebil, M., Benatsou, B., Roche, A., Ducreux, M., Malka, D. & Boige, V. 2011 Advanced hepatocellular carcinoma: early evaluation of response to bevacizumab therapy at dynamic contrast-enhanced US with quantification-preliminary results. *Radiology* **258**, 291–300. (doi:10.1148/radiol.10091870)
18 Staub, D., Partovi, S., Schinkel, A. F. L., Coll, B., Uthoff, H., Aschwanden, M., Jaeger, K. A. & Feinstein, S. B. 2011 Correlation of carotid artery atherosclerotic lesion echogenicity and severity at standard US with intraplaque neovascularization detected at contrast-enhanced US. *Radiology* **258**, 618–626. (doi:10.1148/radiol.10101008)
19 Kamiyama, N., Moriyasu, F., Mine, Y. & Goto, Y. 1999 Analysis of flash echo from contrast agent for designing optimal ultrasound diagnostic systems. *Ultrasound Med. Biol.* **25**, 411–420. (doi:10.1016/S0301-5629(98)00182-3)
20 Blomley, M. J. K., Albrecht, T., Cosgrove, D. O., Eckersley, R. J., Butler-Barnes, J., Jayaram, V. *et al.* 1999 Stimulated acoustic emission to image a late liver and spleen- specific phase of Levovist® in normal volunteers and patients with and without liver disease. *Ultrasound Med. Biol.* **25**, 1341–1352. (doi:10.1016/S0301-5629(99)00081-2)
21 Verbeek, X., Willigers, J. M., Prinzen, F. W., Peschar, M., Ledoux, L. A. F. & Hoeks, A. P. G. 2001 High-resolution functional imaging with ultrasound contrast agents based on RF processing in an *in vivo* kidney experiment. *Ultrasound Med. Biol.* **27**, 223–233. (doi:10.1016/S0301-5629(00)00318-5)
22 Peronneau, P., Lassau, N., Leguerney, I., Roche, A. & Cosgrove, D. 2010 Contrast ultrasonography: necessity of linear data processing for the quantification of tumor vascularization. *Ultraschall in Der Medizin* **31**, 370–378. (doi:10.1055/s-0029-1245450)
23 Koster, J. *et al.* 2001 Blood flow assessment by ultrasound-induced destruction of echocontrast agents using harmonic power Doppler imaging: which parameters determine contrast replenishment curves? *Echocardiogr. J. Cardiovasc. Ultrasound Allied Tech.* **18**, 1–8. (doi:10.1046/j.1540-8175.2001.00001.x)
24 Schlosser, T. *et al.* 2001 Feasibility of the flash-replenishment concept in renal tissue: Which parameters affect the assessment of the contrast replenishment? *Ultrasound Med. Biol.* **27**, 937–944. (doi:10.1016/S0301-5629(01)00397-0)
25 Tang, M. X. & Eckersley, R. J. 2007 Frequency and pressure dependent attenuation and scattering by microbubbles. *Ultrasound Med. Biol.* **33**, 164–168. (doi:10.1016/j.ultrasmedbio.2006.07.031)
26 Emmer, M., Vos, H. J., Goertz, D. E., van Wamel, A., Versluis, M. & de Jong, N. 2009 Pressure-dependent attenuation and scattering of phospholipid-coated microbubbles at low acoustic pressures. *Ultrasound Med. Biol.* **35**, 102–111. (doi:10.1016/j.ultrasmedbio.2008.07.005)
27 Sboros, V., MacDonald, C. A., Pye, S. D., Moran, C. M., Gomatam, J. & McDicken, W. N. 2002 The dependence of ultrasound contrast agents backscatter on acoustic pressure: theory versus experiment. *Ultrasonics* **40**, 579–583. (doi:10.1016/S0041-624X(02)00175-0)
28 Morgan, K. E., Dayton, P. A., Kruse, D. E., Klibanov, A. L., Brandenburger, G. H. & Ferrara, K. W. 1998 Changes in the echoes from ultrasonic contrast agents with imaging

parameters. *IEEE Trans. Ultrason. Ferroelectr. Freq. Control* **45**, 1537–1548. (doi:10.1109/58.738293)
29 Shi, W. T., Forsberg, F., Raichlen, J. S., Needleman, L. & Goldberg, B. B. 1999 Pressure dependence of subharmonic signals from contrast microbubbles. *Ultrasound Med. Biol.* **25**, 275–283. (doi:10.1016/S0301-5629(98)00163-X)
30 Shi, W. T. & Forsberg, F. 2000 Ultrasonic characterization of the nonlinear properties of contrast microbubbles. *Ultrasound Med. Biol.* **26**, 93–104. (doi:10.1016/S0301-5629(99)00117-9)
31 Emmer, M., Van Wamel, A., Goertz, D. E. & De Jong, N. 2007 The onset of microbubble vibration. *Ultrasound Med. Biol.* **33**, 941–949. (doi:10.1016/j.ultrasmedbio.2006.11.004)
32 Tang, M. X. & Eckersley, R. J. 2006 Nonlinear propagation of ultrasound through microbubble contrast agents and implications for imaging. *IEEE Trans. Ultrason. Ferroelectr. Freq. Control* **53**, 2406–2415. (doi:10.1109/TUFFC.2006.189)
33 Gauthier, T. P., Averkiou, M. A. & Leen, E. L. S. 2011 Perfusion quantification using dynamic contrast-enhanced ultrasound: The impact of dynamic range and gain on time-intensity curves. *Ultrasonics* **51**, 102–106. (doi:10.1016/j.ultras.2010.06.004)
34 Averkiou, M., Lampaskis, M., Kyriakopoulou, K., Skarlos, D., Klouvas, G., Strouthos, C. & Leen, E. 2010 Quantification of tumor microvascularity with respiratory gated contrast enhanced ultrasound for monitoring therapy. *Ultrasound Med. Biol.* **36**, 68–77. (doi:10.1016/j.ultrasmedbio.2009.07.005)
35 Cosgrove, D., Eckersley, R., Blomley, M. & Harvey, C. 2001 Quantification of blood flow. *Eur Radiol.* **11**, 1338–1344. (doi:10.1007/s003300100985)
36 Gauthier, T. P., Averkiou, M. A. & Leen, E. L. 2011 Perfusion quantification using dynamic contrast-enhanced ultrasound: the impact of dynamic range and gain on time-intensity curves. *Ultrasonics* **51**, 102–106. (doi:10.1016/j.ultras.2010.06.004)
37 Rognin, N. G., Frinking, P., Costa, M. & Arditi, M. (eds) 2008 *In vivo* perfusion quantification by contrast ultrasound: validation of the use of linearized video data vs. raw RF data. In *Ultrasonics Symp.*, IUS 2008 IEEE, pp. 1690–1693. Piscataway, NJ: IEEE.
38 Hoff, L. (ed.) 2001 *Acoustic characterisation of contrast agents for medical ultrasound imaging*. Dordrecht, The Netherlands: Kluwer Academic Publishers.
39 Tde Jong, N. & Hoff, L. 1993 Ultrasound scattering properties of Albunex microspheres. *Ultrasonics* **31**, 175–181. (doi:10.1016/0041-624X(93)90004-J)
40 Marsh, J. N., Hughes, M. S., Hall, C. S., Lewis, S. H., Trousil, R. L., Brandenburger, G. H., Levene, H. & Miller, J. G. 1998 Frequency and concentration dependence of the backscatter coefficient of the ultrasound contrast agent Albunex (R). *J. Acoust. Soc. Am.* **104**, 1654–1666. (doi:10.1121/1.424378)
41 Bouakaz, A., De Jong, N. & Cachard, C. 1998 Standard properties of ultrasound contrast agents. *Ultrasound Med. Biol.* **24**, 469–472. (doi:10.1016/S0301-5629(97)00290-1)
42 Frinking, P. J. & de Jong, N. 1998 Acoustic modeling of shell-encapsulated gas bubbles. *Ultrasound Med. Biol.* **24**, 523–533. (doi:10.1016/S0301-5629(98)00009-X)
43 Sboros, V., Pye, S. D., Anderson, T. A., Moran, C. M. & McDicken, W. N. 2007 *Acoustic Rayleigh scattering at individual micron-sized bubbles. Appl. Phys. Lett.* **90**, (doi:10.1063/1.2714996)
44 Cameron JRJGSRMG 1999 *Physics of the body*, 2nd edn. Madison, WI: Medical Physics Publishing.
45 Fairbank, W. M. & Scully, M. O. 1977 New noninvasive technique for cardiac pressure measurement—resonant scattering of ultrasound from bubbles. *IEEE Trans. Biomed. Eng.* **24**, 107–110. (doi:10.1109/TBME.1977.326112)
46 Moravi, V., Shroff, S. G., Robinson, K. A., Ng, A. F., Cholley, B. P., Marcus, R. H. & Lang, R. M. 1994 Effects of left-ventricular pressure on sonicated albumin microbubbles—evaluation using an isolated rabbit heart model. *J. Am. Coll. Cardiol.* **24**, 1779–1785. (doi:10.1016/0735-1097(94)90187-2)
47 Leodore, L. A., Forsberg, F. & Shi, W. T. 2007 *In vitro* pressure estimation obtained from subharmonic contrast microbubble signals. *2007 IEEE Ultrason. Symp. Proc.* **1–6**, 2207–2210. (doi:10.1109/ULTSYM.2007.555)
48 Andersen, K. S. & Jensen, J. A. 2010 Non-invasive estimation of blood pressure using ultrasound contrast agents. In *Int. Congress on Ultrasonics, Proc.* (ed. L. G. Garreton), pp. 245–253. Amsterdam, The Netherlands: Elsevier.
49 de Jong, N., Ten Cate, F. J., Vletter, W. B. & Roelandt, J. R. T. C. 1993 Quantification of transpulmonary echocontrast effects. *Ultrasound Med. Biol.* **19**, 279–288. (doi:10.1016/0301-5629(93)90100-3)
50 Shapiro, J. R., Reisner, S. A., Lichtenberg, G. S. & Meltzer, R. S. 1990 Intravenous contrast echocardiography with use of sonicated albumin in humans—systolic disappearance of left-ventricular contrast after transpulmonary transmission. *J. Am. Coll. Cardiol.* **16**, 1603–1607. (doi:10.1016/0735-1097(90)90308-C)
51 Vuille, C., Nidorf, M., Morrissey, R. L., Newell, J. B., Weyman, A. E. & Picard, M. H. 1994 Effect of static pressure on the disappearance rate of specific echocardiographic contrast agents. *J. Am. Soc. Echocardiogr.* **7**, 347–354.
52 Gottlieb, S., Ernst, A. & Meltzer, R. S. 1995 Effect of pressure on echocardiographic videodensity from sonicated albumin—an *in vitro* model. *J. Ultrasound Med.* **14**, 109–116.
53 Brayman, A. A., Azadniv, M., Miller, M. W. & Meltzer, R. S. 1996 Effect of static pressure on acoustic transmittance of Albunex(R) microbubble suspensions. *J. Acoust. Soc. Am.* **99**, 2403–2408. (doi:10.1121/1.415428)
54 Gandhok, N. K., Block, R., Ostoic, T., Rawal, M., Hickle, P., Devries, S. & Feinstein, S. 1997 Reduced forward output states affect the left ventricular opacification of intravenously administered Albunex. *J. Am. Soc. Echocardiogr.* **10**, 25–30. (doi:10.1016/S0894-7317(97)80029-6)
55 Lindner, J. R., Song, J., Jayaweera, A. R., Sklenar, J. & Kaul, S. 2002 Microvascular rheology of definity microbubbles after intra-arterial and intravenous administration. *J. Am. Soc. Echocardiogr.* **15**, 396–403. (doi:10.1067/mje.2002.117290)
56 Bouakaz, A. & de Jong, N. 2007 WFUMB safety symposium on echo-contrast agents: nature and types of ultrasound contrast agents. *Ultrasound Med. Biol.* **33**, 187–196. (doi:10.1016/j.ultrasmedbio.2006.07.008)
57 Vanliew, H. D. & Burkard, M. E. 1995 Bubbles in circulating blood—stabilization and simulations of cyclic changes of size and content. *J. Appl. Physiol.* **79**, 1379–1385.
58 Maresca, D., Emmer, M., van Neer, P. L. M. J., Vos, H. J., Versluis, M., Muller, M., de Jong, N. & van der Steen, A. F. W. 2010 Acoustic sizing of an ultrasound contrast agent. *Ultrasound Med. Biol.* **36**, 1713–1721. (doi:10.1016/j.ultrasmedbio.2010.06.014)
59 Blomley, M. J. K. *et al.* 1999 Stimulated acoustic emission to image a late liver and spleen-specific phase of Levovist® in normal volunteers and patients with and without liver disease. *Ultrasound Med. Biol.* **25**, 1341–1352. (doi:10.1016/S0301-5629(99)00081-2)

60 Lim, A. K. P., Patel, N., Eckersley, R. J., Goldin, R. D., Thomas, H. C., Cosgrove, D. O., Taylor-Robinson, S. D. & Blomley, M. J. K. 2006 Hepatic vein transit time of SonoVue: a comparative study with Levovist. *Radiology* **240**, 130–135. (doi:10.1148/radiol.2401041517)

61 Owen, D. R., Shalhoub, J., Miller, S., Gauthier, T., Doryforou, O., Davies, A. H. & Leen, E. L. S. 2010 Inflammation within carotid atherosclerotic plaque: assessment with late-phase contrast-enhanced US. *Radiology* **255**, 638–644. (doi:10.1148/radiol.10091365)

62 Kono, Y., Steinbach, G. C., Peterson, T., Schmid-Schonbein, G. W. & Mattrey, R. F. 2002 Mechanism of parenchymal enhancement of the liver with a microbubble-based US contrast medium: an intravital microscopy study in rats. *Radiology* **224**, 253–257. (doi:10.1148/radiol.2241011352)

63 Lindner, J. R., Dayton, P. A., Coggins, M. P., Ley, K., Song, J., Ferrara, K. & Kaul, S. 2000 Noninvasive imaging of inflammation by ultrasound detection of phagocytosed microbubbles. *Circulation* **102**, 531–538.

64 Yanagisawa, K., Moriyasu, F., Miyahara, T., Yuki, M. & Iijima, H. 2007 Phagocytosis of ultrasound contrast agent microbubbles by Kupffer cells. *Ultrasound Med. Biol.* **33**, 318–325. (doi:10.1016/j.ultrasmedbio.2006.08.008)

65 Shunichi, S., Hiroko, I., Fuminori, M. & Waki, H. 2009 Definition of contrast enhancement phases of the liver using a perfluoro-based microbubble agent, perflubutane microbubbles. *Ultrasound Med. Biol.* **35**, 1819–1827. (doi:10.1016/j.ultrasmedbio.2009.05.013)

66 Lee, K. H., Choi, B. I., Kim, K. W., Kim, J. S., Won, H. J., Han, J. K., Kim, S. H. & Park, S. H. 2003 Contrast-enhanced dynamic ultrasonography of the liver: optimization of hepatic arterial phase in normal volunteers(2). *Abdom. Imaging* **28**, 652–656. (doi:10.1007/s00261-002-0092-5)

67 Gasparini, C., Bertolotto, M., Crocè, S. L., Perrone, R., Quaia, E. & Tiribelli, C. 2003 Evaluation of liver parenchymal blood flow with contrast-enhanced US: preliminary results in healthy and cirrhotic patients1. *Acad. Radiol.* **10**, 869–876. (doi:10.1016/S1076-6332(03)00003-5)

68 Maruyama, H., Matsutani, S., Saisho, H., Mine, Y., Yuki, H. & Miyata, K. 2004 Different behaviors of microbubbles in the liver: time-related quantitative analysis of two ultrasound contrast agents, Levovist® and Definity®. *Ultrasound Med. Biol.* **30**, 1035–1040. (doi:10.1016/j.ultrasmedbio.2004.06.008)

69 Quaia, E., Blomley, M. J. K., Patel, S., Harvey, C. J., Padhani, A., Price, P. & Cosgrove, D. O. 2002 Initial observations on the effect of irradiation on the liver-specific uptake of Levovist. *Eur. J. Radiol.* **41**, 192–199. (doi:10.1016/S0720-048X(01)00458-2)

70 Liu, G. J., Moriyasu, F., Hirokawa, T., Rexiati, M., Yamada, M. & Imai, Y. 2008 Optical microscopic findings of the behavior of perflubutane microbubbles outside and inside Kupffer cells during diagnostic ultrasound examination. *Invest. Radiol.* **43**, 829–836. (doi:10.1097/RLI.0b013e3181852719)

71 Skrok, J. 2007. Markedly increased signal enhancement after the second injection of SonoVue® compared to the first—a quantitative normal volunteer study. In *12th European Symp. on Ultrasound Contrast Imaging, January 25–26th, 2007*, Rotterdam, The Netherlands (Conference presentation).

72 Uchimoto, R., Niwa, K., Eguchi, H., Kamiyama, N., Mine, Y., Miyazawa, T. & Brautigam, M. 1999 *In vivo* kinetics of microbubbles of SHU 508 A (Levovist((R))): comparison with Indocyanine Green in rabbits. *Ultrasound Med. Biol.* **25**, 1365–1370. (doi:10.1016/S0301-5629(99)00090-3)

73 Mullin, L., Gessner, R., Kwan, J., Borden, M. A. & Dayton, P. A. (eds) 2009. An *in vivo* evaluation of the effects of anesthesia carrier gases on ultrasound contrast agent circulation. In *Ultrasonics Symp. (IUS), 2009 IEEE Int., 20–23 September 2009*. New York, NY: IEEE.

74 Izumi, H. & Ito, Y. 1999 Correlation between degree of inhibition of parasympathetic reflex vasodilation and MAC value for various inhalation anesthetics. *Gen. Pharmacol.* **32**, 689–693. (doi:10.1016/S0306-3623(98)00242-0)

75 Molina, R., Sánchez, M., Hidalgo, A. & JoséGarcía De Boto, M. 1995 Effects of preanesthetic and anesthetic drugs on endothelium-dependent responses in the rat aorta. *Gen. Pharmacol. Vasc. Syst.* **26**, 169–175. (doi:10.1016/0306-3623(94)00145-D)

76 Nyman, H. T., Kristensen, A. T., Kjelgaard-Hansen, M. & McEvoy, F. J. 2005 Contrast-enhanced ultrasonography in normal canine liver. Evaluation of imaging and safety parameters. *Vet. Radiol. Ultrasound* **46**, 243–250. (doi:10.1111/j.1740-8261.2005.00034.x)

77 Feingold, S., Gessner, R., Guracar, I. M. & Dayton, P. A. 2010 Quantitative volumetric perfusion mapping of the microvasculature using contrast ultrasound. *Invest. Radiol.* **45**, 669–674. (doi:10.1097/RLI.0b013e3181ef0a78)

78 Leinonen, M. R., Raekallio, M. R., Vainio, O. M., Ruohoniemi, M. O. & O'Brien, R. T. 2011 The effect of the sample size and location on contrast ultrasound measurement of perfusion parameters. *Vet. Radiol. Ultrasound* **52**, 82–87.

79 Duck, F. A. 1990 *Physical properties of tissue: a comprehensive reference book*. London, UK: Academic Press.

80 Maklad, N. F., Ophir, J. & Balsara, V. 1984 Attenuation of ultrasound in normal liver and diffuse liver disease *in vivo*. *Ultrasonic Imaging* **6**, 117–125. (doi:10.1016/0161-7346(84)90019-1)

81 Bos, L. J., Piek, J. J. & Spaan, J. A. E. 1996 Effects of shadowing on the time–intensity curves in contrast echocardiography: a phantom study. *Ultrasound Med. Biol.* **22**, 217–227. (doi:10.1016/0301-5629(95)02032-2)

82 Tang, M. X., Mari, J. M., Wells, P. N. T. & Eckersley, R. J. 2008 Attenuation correction in ultrasound contrast agent imaging: elementary theory and preliminary experimental evaluation. *Ultrasound Med. Biol.* **34**, 1998–2008. (doi:10.1016/j.ultrasmedbio.2008.04.008)

83 Lindner, J. R. & Sklenar, J. 2004 Placing faith in numbers: quantification of perfusion with myocardial contrast echocardiography. *J. Am. Coll. Cardiol.* **43**, 1814–1816. (doi:10.1016/j.jacc.2004.03.002)

84 Yano, A., Ito, H., Iwakura, K., Kimura, R., Tanaka, K., Okamura, A., Kawano, S., Masuyama, T. & Fujii, K. 2004 Myocardial contrast echocardiography with a new calibration method can estimate myocardial viability in patients with myocardial infarction. *J. Am. Coll. Cardiol.* **43**, 1799–1806. (doi:10.1016/j.jacc.2003.10.069)

85 Tang, M. X., Eckersley, R. J. & Noble, J. A. 2005 Pressure-dependent attenuation with microbubbles at low mechanical index. *Ultrasound Med. Biol.* **31**, 377–384. (doi:10.1016/j.ultrasmedbio.2004.12.009)

86 Pellot-Barakat, C., Mule, S., De Cesare, A., Lamuraglia, M., Lucidarme, O., Bridal, L., Herment, A. & Frouin, F. 2009 FAMIS based evaluation of a regularized attenuation correction method in contrast ultrasound imaging. *Irbm* **30**, 174–178. (doi:10.1016/j.irbm.2009.05.002)

87 Mule, S., De Cesare, A., Lucidarme, O., Frouin, F. & Herment, A. 2008 Regularized estimation of contrast agent attenuation to improve the imaging of microbubbles in small animal studies. *Ultrasound Med. Biol.* **34**, 938–948. (doi:10.1016/j.ultrasmedbio.2007.11.014)

88 Mari, J. M., Hibbs, K. & Tang, M. X. 2007 A non-linear ultrasonic scattering approach for micro bubble concentration quantification. *2007 Annu. Int. Conf. IEEE Eng. Med. Biol. Soc.* **1–16**, 2183–2186. (doi:10.1109/IEMBS.2007.4352756)

89 Mari, J. M., Hibbs, K., Stride, E., Eckersley, R. J. & Tang, M. X. 2010 An approximate nonlinear model for time gain compensation of amplitude modulated images of ultrasound contrast agent perfusion. *IEEE Trans. Ultrason. Ferroelectr. Freq. Control* **57**, 818–829. (doi:10.1109/TUFFC.2010.1487)

90 Tang, M.-X., Kamiyama, N. & Eckersley, R. J. 2010 Effects of nonlinear propagation in ultrasound contrast agent imaging. *Ultrasound Med. Biol.* **36**, 459–466. (doi:10.1016/j.ultrasmedbio.2009.11.011)

91 Stride, E., Tang, M. X. & Eckersley, R. J. 2009 Physical phenomena affecting quantitative imaging of ultrasound contrast agents. *Appl. Acoust.* **70**, 1352–1362. (doi:10.1016/j.apacoust.2008.10.003)

92 Yu, H. J., Jang, H. J., Kim, T. K., Khalili, K., Williams, R., Lueck, G., Hudson, J. & Burns, P. N. 2010 pseudoenhancement within the local ablation zone of hepatic tumors due to a nonlinear artifact on contrast-enhanced ultrasound. *Am. J. Roentgenol.* **194**, 653–659. (doi:10.2214/AJR.09.3109)

93 Pasovic, M., Danilouchkine, M., Matte, G., van der Steen, A. F. W., Basset, O., de Jong, N. & Cachard, C. 2010 Broadband reduction of the second harmonic distortion during nonlinear ultrasound wave propagation. *Ultrasound Med. Biol.* **36**, 1568–1580. (doi:10.1016/j.ultrasmedbio.2010.06.006)

94 Couture, O., Aubry, J. F., Montaldo, G., Tanter, M. & Fink, M. 2008 Suppression of tissue harmonics for pulse-inversion contrast imaging using time reversal. *Phys. Med. Biol.* **53**, 5469–5480. (doi:10.1088/0031-9155/53/19/013)

95 Liao, A. H., Shen, C. C. & Li, P. C. 2010 Potential contrast improvement in ultrasound pulse inversion imaging using EMD and EEMD. *IEEE Trans. Ultrason. Ferroelectr. Freq. Control* **57**, 317–326. (doi:10.1109/TUFFC.2010.1412)

96 Hibbs, K., Mari, J. M., Stride, E., Eckersley, R. J., Noble, A. & Tang, M. X. 2007 Nonlinear propagation of ultrasound through microbubble clouds: a novel numerical implementation. *2007 IEEE Ultrason. Symp. Proc.* **1–6**, 1997–2000. (doi:10.1109/ULTSYM.2007.502)

97 Tang, M.-X., Loughran, J., Stride, E., Zhang, D. & Eckersley, R. J. 2011 Effect of bubble shell nonlinearity on ultrasound nonlinear propagation through microbubble populations. *J. Acoust. Soc. Am.* **129**, EL76–EL82. (doi:10.1121/1.3544677)

98 O'Brien, J.-P., Stride, E., Ovenden, N., Tang, M.-X. & Eckersley, R. J. 2011 Nonlinear propagation models for ultrasound pulse propagation through a polydisperse bubble population. In *The 16th European Symp. on Ultrasound Contrast Imaging, Rotterdam.* Rotterdam, The Netherlands: Erasmus Medical Centre.

99 Lim, A., Patel, N., Eckersley, R., Taylor-Robinson, S., Martin, B. & David, C. 2003 Differences in the liver kinetics of SonoVue and Levovist. *Ultrasound Med. Biol.* **29**, S11–S12. (doi:10.1016/S0301-5629(03)00110-8)

100 Sboros, V., Moran, C. M., Pye, S. D. & McDicken, W. N. 2001 Contrast agent stability: a continuous B-mode imaging approach. *Ultrasound Med. Biol.* **27**, 1367–1377. (doi:10.1016/S0301-5629(01)00440-9)

101 Grulke, D. C., Marsh, N. A. & Hills, B. A. 1973 Experimental air-embolism—measurement of microbubbles using coulter counter. *Br. J. Exp. Pathol.* **54**, 684–691.

102 Sennoga, C. A., Mahue, V., Loughran, J., Casey, J., Seddon, J. M., Tang, M. & Eckersley, R. J. 2010 On sizing and counting of microbubbles using optical microscopy. *Ultrasound Med. Biol.* **36**, 2093–2096. (doi:10.1016/j.ultrasmedbio.2010.09.004)

103 Bloch, S. H., Short, R. E., Ferrara, K. W. & Wisner, E. R. 2005 The effect of size on the acoustic response of polymer-shelled contrast agents. *Ultrasound Med. Biol.* **31**, 439–444. (doi:10.1016/j.ultrasmedbio.2004.12.016)

104 de Jong, N., Hoff, L., Skotland, T. & Bom, N. 1992 Absorption and scatter of encapsulated gas filled microspheres—theoretical considerations and some measurements. *Ultrasonics* **30**, 95–103. (doi:10.1016/0041-624X(92)90041-J)

105 Hasik, M. J., Kim, D. H., Howle, L. E., Needham, D. & Prush, D. P. 2002 Evaluation of synthetic phospholipid ultrasound contrast agents. *Ultrasonics* **40**, 973–982. (doi:10.1016/S0041-624X(02)00384-0)

106 Kudo, N. & Yamamoto, K. 2004 Physical properties of ultrasound contrast agents. *Int. Cong. Ser.* **1274**, 49–52. (doi:10.1016/j.ics.2004.07.024)

107 Stride, E. 2008 The influence of surface adsorption on microbubble dynamics. *Phil. Trans. R. Soc. A* **366**, 2103–2115. (doi:10.1098/rsta.2008.0001)

108 Fisher, N. G., Christiansen, J. P., Klibanov, A., Taylor, R. P., Kaul, S. & Lindner, J. R. 2002 Influence of microbubble surface charge on capillary transit and myocardial contrast enhancement. *J. Am. Coll. Cardiol.* **40**, 811–819. (doi:10.1016/S0735-1097(02)02038-7)

109 Wrenn, S. P., Mleczko, M. & Schmitz, G. 2009 Phospholipid-stabilized microbubbles: influence of shell chemistry on cavitation threshold and binding to giant uni-lamellar vesicles. *Appl. Acoust.* **70**, 1313–1322. (doi:10.1016/j.apacoust.2008.09.017)

110 Borden, M. A., Dayton, P., Shukui, Z. & Ferrara, K. W. (eds) 2004 Physico-chemical properties of the microbubble lipid shell [ultrasound contrast agents]. In *Ultrasonics Symp., 2004 IEEE.* New York, NY: IEEE.

111 Borden, M. A., Kruse, D. E., Caskey, C. F., Zhao, S. K., Dayton, P. A. & Ferrara, K. W. (eds) 2004. Influence of lipid shell physicochemical properties on ultrasound-induced microbubble destruction. In *Meeting of the IEEE-Ultrasonics-Ferroelectrics-and-Frequency-Control-Society, 2005.* Montreal, Canada: IEEE Institute of Electrical Electronics Engineers Inc.

112 Borden, M. A. & Longo, M. L. 2002 Dissolution behavior of lipid monolayer-coated, air-filled microbubbles. Effect of lipid hydrophobic chain length. *Langmuir* **18**, 9225–9233.

113 Chen, W.-S., Matula, T. J. & Crum, L. A. 2002 The disappearance of ultrasound contrast bubbles: observations of bubble dissolution and cavitation nucleation. *Ultrasound Med. Biol.* **28**, 793–803. (doi:10.1016/S0301-5629(02)00517-3)

114 Raisinghani, A. & DeMaria, A. N. 2002 Physical principles of microbubble ultrasound contrast agents. *Am. J. Cardiol.* **90**, 3–7. (doi:10.1016/S0002-9149(02)02858-8)

115 Uchimoto, R., Niwa, K., Tsuda, N., Miyazawa, T. & Bräutigam, M. 2000 Comparison of the efficacy of two air-based contrast agents in dogs. *Eur. J. Ultrasound* **11**, 127–133. (doi:10.1016/S0929-8266(00)00079-3)

116 Bokor, D. 2000 Diagnostic efficacy of SonoVue. *Am. J. Cardiol.* **86**, 19–24. (doi:10.1016/S0002-9149(00)00985-1)

117 Mulvana, H., Stride, E., Hajnal, J. V. & Eckersley, R. J. 2010 Temperature dependent behavior of ultrasound contrast agents. *Ultrasound Med. Biol.* **36**, 925–934. (doi:10.1016/j.ultrasmedbio.2010.03.003)

118 Chlon, C., Guedon, C., Verhaagen, B., Shi, W. T., Hall, C. S., Lub, J. & Böhmer, M. R. 2009 Effect of molecular weight, crystallinity, and hydrophobicity on the acoustic activation of polymer-shelled ultrasound contrast agents. *Biomacromolecules* **10**, 1025–1031. (doi:10.1021/bm801243u)

119 Andersen, K. S. & Jensen, J. A. 2009 Ambient pressure sensitivity of microbubbles investigated through a parameter study. *J. Acoust. Soc. Am.* **126**, 3350–3358. (doi:10.1121/1.3242359)

120 Talu, E., Powell, R. L., Longo, M. L. & Dayton, P. A. 2008 Needle size and injection rate impact microbubble contrast agent population. *Ultrasound Med. Biol.* **34**, 1182–1185. (doi:10.1016/j.ultrasmedbio.2007.12.018)

121 Barrack, T. & Stride, E. 2009 Microbubble destruction during intravenous administration: a preliminary study. *Ultrasound Med. Biol.* **35**, 515–522. (doi:10.1016/j.ultrasmedbio.2008.07.008)

122 Browning, R. M., H; Wells, D. J. & ; Eckersley, R. J. Effect of needle gauge on microbubble mediated cell transfection *in vivo*. In *British Medical Ultrasound General Scientific Meeting* (*Conference presentation*), *28–30 September 2010*. London, UK: British medical Ultrasound Society.

123 Palmowski, M., Lederle, W., Gaetjens, J., Socher, M., Hauff, P., Bzyl, J., Semmler, W., Günther, R. W. & Kiessling, F. 2010 Comparison of conventional time-intensity curves vs. maximum intensity over time for post-processing of dynamic contrast-enhanced ultrasound. *Eur. J. Radiol.* **75**, e149–e153. (doi:10.1016/j.ejrad.2009.10.030)

124 Duncan, P. B. & Needham, D. 2004 Test of the Epstein–Plesset model for gas microparticle dissolution in aqueous media: effect of surface tension and gas undersaturation in solution. *Langmuir* **20**, 2567–2578. (doi:10.1021/la034930i)

125 Katiyar, A., Sarkar, K. & Jain, P. 2009 Effects of encapsulation elasticity on the stability of an encapsulated microbubble. *J. Colloid Interface Sci.* **336**, 519–525. (doi:10.1016/j.jcis.2009.05.019)

126 Kwan, J. J. & Borden, M. A. 2010 Microbubble dissolution in a multigas environment. *Langmuir* **26**, 6542–6548. (doi:10.1021/la904088p)

127 Stride, E. & Saffari, N. 2005 Investigating the significance of multiple scattering in ultrasound contrast agent particle populations. *Ultrason. Ferroelectr. Freq. Control IEEE Trans.* **52**, 2332–2345. (doi:10.1109/TUFFC.2005.1563278)

128 Lampaskis, M. & Averkiou, M. 2010 investigation of the relationship of nonlinear backscattered ultrasound intensity with microbubble concentration at low MI. *Ultrasound Med. Biol.* **36**, 306–312. (doi:10.1016/j.ultrasmedbio.2009.09.011)

129 Porter, T., Kricsfeld, D., Cheatham, S. & Li, S. 1998 Effect of blood and microbubble oxygen and nitrogen content on perfluorocarbon-filled dextrose albumin microbubble size and efficacy: *in vitro* and *in vivo* studies. *J. Am. Soc. Echocardiogr.* **11**, 421–425. (doi:10.1016/S0894-7317(98)70020-3)

130 Rubaltelli, L., Corradin, S., Dorigo, A., Tregnaghi, A., Adami, F., Rossi, C. R. & Stramare, R. 2007 Automated quantitative evaluation of lymph node perfusion on contrast-enhanced sonography. *Am. J. Roentgenol.* **188**, 977–983. (doi:10.2214/AJR.06.0562)

131 Eckersley, R. J., Sedelaar, J. P. M., Blomley, M. J. K., Wijkstra, H., deSouza, N. M., Cosgrove, D. O. & de la Rosette, J. J. M. C. H. 2002 Quantitative microbubble enhanced transrectal ultrasound as a tool for monitoring hormonal treatment of prostate carcinoma. *Prostate* **51**, 256–267. (doi:10.1002/pros.10065)

132 Hettiarachchi, K., Talu, E., Longo, M. L., Dayton, P. A. & Lee, A. P. 2007 On-chip generation of microbubbles as a practical technology for manufacturing contrast agents for ultrasonic imaging. *Lab Chip* **7**, 463–468. (doi:10.1039/b701481n)

133 Stride, E. & Edirisinghe, M. 2008 Novel microbubble preparation technologies. *Soft Matter* **4**, 2350–2359. (doi:10.1039/b809517p)

134 Lin, P. L., Eckersley, R. J. & Hall, E. A. H. 2009 Ultrabubble: a laminated ultrasound contrast agent with narrow size range. *Adv. Mater.* **21**, 3949–3952.